Climatology of aerosol components concentration derived by GRASP algorithm from multi-angular polarimetric POLDER-3 observations

5 Lei Li[1], Yevgeny Derimian[2], Cheng Chen[2,3], Xindan Zhang[1], Huizheng Che[1*], Gregory L. Schuster[4], David Fuertes[3], Pavel Litvinov[3], Tatyana Lapyonok[2], Anton Lopatin[3], Christian Matar[3], Fabrice Ducos[2], Yana Karol[3], Benjamin Torres[2], Ke Gui[1], Yu Zheng[1], Yuanxin Liang[1], Yadong Lei[1], Jibiao Zhu[1], Lei Zhang[1], Junting Zhong[1], Xiaoye Zhang[1], Oleg Dubovik[2*]

[1]State Key Laboratory of Severe Weather (LASW) and Key Laboratory of Atmospheric Chemistry (LAC), Chinese Academy of Meteorological Sciences, CMA, Beijing, 100081, China
[2]Univ. Lille, CNRS, UMR 8518 - LOA - Laboratoire d'Optique Atmosphérique, F-59000 Lille, France
[3]GRASP-SAS, Villeneuve d'Ascq, France
15 [4]NASA Langley Research Center, Hampton, VA, USA

Correspondence to: Huizheng Che (chehz@cma.gov.cn) and Oleg Dubovik (oleg.dubovik@univ-lille.fr)

Abstract. The study presents a climatology of aerosol composition concentration obtained by a recently
20 developed GRASP/Component (GRASP stands for the Generalized Retrieval of Atmosphere and Surface Properties algorithm) approach applied to the whole archive of POLDER-3 (POLarization and Directionality of the Earth's Reflectances) observations. The conceptual specific of the GRASP/Component approach is in direct retrieval of aerosol speciation (component fraction) without an intermediate retrievals of aerosol optical characteristics. Despite a global validation of the derived aerosol
25 component product is challenging, the results obtained are in line with general knowledge about aerosol types in different regions. In addition, we compare the GRASP derived black carbon and dust components

with those of the MERRA-2 (Modern-Era Retrospective Analysis for Research and Applications, version 2) product. Quite reasonable general agreement in spatial and temporal distribution of the species provided by GRASP and MERRA-2 was found, the differences however appeared in regions known for strong biomass burning and dust emissions; the reasons for the discrepancies are discussed. The other derived components, such as ~~concentration~~ concentrations of absorbing (black carbon, brown carbon, iron oxides content in mineral dust) and scattering (ammonium sulphate and nitrate, organic carbon, non-absorbing dust) ~~aerosol~~ aerosols, represent scarce but imperative information for validation and potential adjustment of chemical transport models. The aerosol optical properties (e.g., aerosol optical depth, Ångström exponent, single-scattering albedo, fine- and coarse-mode aerosol optical depth) derived by GRASP/Component were found to agree well with the AERONET (Aerosol Robotic Network) ground reference data and fully consistent with the previous GRASP Optimized, High Precision and Models retrieval versions applied to POLDER-3 data. Thus, the presented extensive climatology product provides an opportunity for understanding variabilities and trends in global and regional distributions of aerosol species. The climatology of the aerosol components obtained in addition to the aerosol optical properties provides additional valuable, qualitatively new inside about aerosol distributions and, therefore, demonstrates advantages of multi-angular polarimetric satellite observations as the next frontier for aerosol inversion from advanced satellite observations. The extensive satellite-based aerosol component dataset is expected to be useful for improving global aerosol emissions and component-resolved radiative forcing estimations. The GRASP/Component products are publicly available (https://www.grasp-open.com/products/, last access: 15 March 2022) and the dataset used in the current study is registedred under https://doi.org/10.5281/zenodo.6395384 (Li et al., 2022).

1 Introduction

The latest IPCC (Intergovernmental Panel on Climate Change) have reported that aerosols are still the most contributor to the large forcing uncertainty (Forster et al., 2021) with the assessment of -2.0 and -0.4 W/m^2 (90% likelihood) for the aerosol effective radiative forcing (Bellouin et al., 2020). One of the main factors responsible for the large aerosol radiative forcing uncertainty is the lack of understanding

and knowledge on global aerosol composition distribution. The potential of using remote sensing observations has already demonstrated in several studies. For example, Dubovik et al. (2002b) discussed

55 the differences of spectral absorption between carbonaceous particles and mineral dust using retrieval from the global AERONET (Aerosol Robotic Network) measurements. Schuster et al. (2005), for the first time, demonstrated a potential to infer the black carbon (BC) content from remote sensing AERONET data using an assumption that all aerosol absorption could be interpreted to the contribution of BC component. Then, the hematite and brown carbon (BrC) proportions were successfully estimated by

60 Koven and Fung (2006) and Arola et al. (2011), respectively, from AERONET products using the spectral variability of themselves complex refraction indices. Derimian et al. (2008) discussed the difficulties in the separation of carbonaceous species absorption from mineral dust (largely iron oxides) absorption and highlighted ~~the importance of having sufficient spectral resolution of measurements to capture the differences~~ the importances of sufficient spectral resolution of measurements on captureing the

65 differences in absorption spectral dependence among BC, BrC, and iron oxides are essential for determination of BC, BrC, and iron oxides proportions. With additional constraints on spectral single scattering albedo and the complex refractive index (Arola et al., 2011; Koven and Fung, 2006; Schuster et al., 2005), the proportions of BC, BrC and dust can be estimated simultaneously based on AERONET products (Wang et al., 2013). Recently, Schuster et al. (2016) successfully retrieved the proportions of

70 aerosol absorbing components (BC, BrC, and iron oxides) in fine- and coarse-mode particles of biomass burning and dust aerosols over the globe based on the aerosol products (aerosol size distributions and complex refraction index) provided in the AERONET retrievals described by Dubovik and King (2000) and Dubovik et al. (2002b, 2006). The estimation of aerosol compositional content based on AERONET optical retrievals are also discussed in several other studies (Bahadur et al., 2012; Cazorla et al., 2013;

75 Chung et al., 2012; Costabile et al., 2013; Dey et al., 2006; Li et al., 2013, 2015; Russell et al., 2010; Xie et al., 2014, 2017; Zhang et al., 2018). AERONET products (such as particle size distribution, wavelength dependence of extinction, single scattering albedo) are also used to distinguish the aerosol types at several regional sites (Giles et al., 2012; Logan et al., 2013). The AERONET-derived aerosol properties together with the active measurements of lidar ratio and spectral depolarization ratio also were used by Burton et

80 al. (2012, 2014) for aerosol types classification from the airborne High Spectral Resolution Lidar (HSRL)

measurements. Ganguly et al. (2009a, 2009b) retrieved the concentration of several aerosol components from the combination of AERONET sun photometer and lidar measurements. It is noted that the evaluation of aerosol components by all above approaches are conducted using the remote sensing measurements at several discrete sites even for the globally distributed ground-based AERONET sites.

85

Satellite remote sensing was extensively used in diverse efforts for improving global aerosol monitoring: for characterizing spatial aerosol distribution (Kaufman et al., 2002; Remer et al., 2008), data assimilation (Dubovik et al., 2008; Chen et al., 2018, 2019; Zhang et al., 2008; Shi et al., 2013) and modeling of aerosol climate effects (Bellouin et al., 2005; Jia et al., 2021; Myhre, 2009; Yu et al., 2006), etc.. A variety

90 of inversion algorithms have been proposed and applied to different ~~and sometimes the same~~ space-borne instruments for further understanding of the atmospheric aerosol properties on large spatial scale (Bréon et al., 2011; Dubovik et al., 2019; King et al., 1999; Li et al., 2009). Specifically, a new cloud and haze detection algorithm was proposed for the geostationary satellite Himawari-8 Advanced Himawari Imager (AHI) measurements (Shang et al., 2017, 2019), which had been used for the analysis of diurnal variations

95 of haze weather and the impact of aerosol optical depth (AOD) on the estimation of cloud properties and surface shortwave radiation (Letu et al., 2019, 2020). Sometimes different algorithms are proposed for the same space-borne instruments. For example, Dark Target (DT) (Levy et al., 2013; Remer et al., 2005, 2020), Deep Blue (DB) (Hsu et al., 2006, 2013), and Multi-Angle Implementation of Atmospheric Correction (MAIAC) (Lyapustin et al., 2018) are proposed for inverting the Moderate Resolution Imaging

100 Spectroradiometer (MODIS) observations. All these algorithms enforced the MODIS retrieval and made MODIS aerosol data base a reference aerosol product in the community. At the same time, MODIS a single-view instrument and generally does not provide sufficient information to identify aerosol types. In contrast, the multi-angular intensity observations by MISR (Multiangle Imaging Spectroradiometer) have been used successfully to identify aerosol type in several regional-scale studies including wildfire smoke

105 (Chen et al., 2008; Guo et al., 2013), desert dust (Guo et al., 2013; Kahn et al., 2009), volcanic ash (Kahn and Limbacher, 2012; Scollo et al., 2012; Flower and Kahn, 2017, 2018, 2020, 2021). Nonetheless, although the aerosol classification from MISR data sets has been supported by above mentioned studies these studies provided mainly qualitative flagging of aerosol types for observed aerosol events. In addition,

because of the aerosol types defined by aerosol parameters in the ~~look-up table~~ Look-Up Table (LUT),
the best fit to the observations for intermediate retrievals were obtained using discrete set of possible solutions. In this regards, the numerous studies suggested that multi-angle polarization measurements ~~has~~ have very high information content and are most appropriate for providing potentially for advanced aerosol product enhanced inside about aerosol microphysics and composition (Hasekamp and Landgraf, 2007; Knobelspiesse et al., 2011; Mishchenko and Geogdzhayev, 2007; Mishchenko and Travis, 1997; Tanré et al., 2011). However, due to rather limited amount of available multi-angle polarization observations and the complexity in their interpretation, the added value of satellite polarimetry on aerosol monitoring remains questionable. ~~the impact of satellite polarimetry on aerosol monitoring remains fairly.~~ Indeed, the polarimetry has enhanced sensitivities to numerous atmospheric parameters and inversion algorithms are required to consider all these sensitivities adequately. Partially due to this complexity, the practical advantages of multi-angular polarimetric retrieval were not convincingly exhibited by the available operational multi-angular polarimetric products in the past for a long time and only recently the advanced aerosol products (including present study) make the advantages of the polarimetry for aerosol remote sensing more evident (e.g., see discussion in Dubovik et al., 2019, 2021b). Nonetheless, as discussed by Dubovik et al. (2019, 2021b) there is large number of multi-angle polarimeter missions is planned and significant progress has been achieved in development of the algorithms of new generation for interpretation polarimetry observation. Therefore, the impact of polarimetric data on overall aerosol science is expected to increase rapidly in coming years.

The POLDER (PoLarization and Directionality of the Earth's Reflectances) instrument was a satellite polarimeter designed for collecting the spectral directional polarized solar radiation measurements (Deschamps et al., 1994). POLDER-3, which was launched onboard PARASOL (Polarization & Anisotropy of Reflectances for Atmospheric Sciences coupled with Observations from a Lidar), provided the longest records of multi-angle polarized measurements from March 2005 to October 2013. In order to invert the POLDER multi-angle polarized measurements, several algorithms following the idea of a conventional MODIS-like look-up-table (LUT) approach (Kaufman et al., 1997; Tanré et al., 1997) were originally proposed to retrieve AOD product over ocean (Deuzé et al., 2001; Goloub et al., 1999; Herman

et al., 2005) and fine-mode AOD (AODF) over land (Deuzé et al., 2001; Herman et al., 2005). However, the exploration of the full extent of the aerosol information contained in ~~MAP~~ multi-angular polarimetric (MAP) measurements, start to be feasible only relatively recently with the development of the so-called

140 satellite "algorithms of new generation", such as the SRON (Netherlands Institute for Space Research) (Fu and Hasekamp, 2018; Hasekamp et al., 2011) and GRASP (Dubovik et al., 2011, 2021a) retrievals. These algorithms consider a continuous space of aerosol microphysical properties (size distribution, refractive index), instead of using standard aerosol models, and retrieve the parameters of underlying surface simultaneously with aerosol properties to properly account for land or ocean reflection.

145 Specifically, the data analysed in this paper were generated in frame of algorithm named GRASP (Generalized Retrieval of Atmosphere and Surface Properties), that was initially developed for enhanced retrieval of aerosol properties from POLDER observations (Dubovik et al., 2011) and then the applicability of GRASP has extended to wide variety of diverse remote sensing applications including both passive and active observations (see details in the papers by Dubovik et al., 2014, 2021a). After

150 about a decade of development and advancement, GRASP algorithm has been adapted for operational generation extended aerosol products from POLDER observations. Several data sets of enhance aerosol retrieval from POLDER observations (see Section 4 in Dubovik et al., 2021a) that now are publicly available (archived at the AERIS/ICARE Data and Services Center (http://www.icare.univ-lille1.fr) and GRASP-OPEN site (https://www.grasp-open.com). All POLDER/GRASP retrieval releases include

155 extended set of conventional aerosol optical parameters (such as spectral aerosol optical depth, spectral aerosol absorption optical depth, spectral fine-mode aerosol optical depth, spectral coarse-mode aerosol optical depth, particle size distribution, single-scattering albedo, complex refractive index, fraction of spherical particles, etc.) (Chen et al., 2020). In addition, the latest POLDER-3/GRASP-Component processing provided also some information of aerosol composition by estimation of fractions of the such

160 aerosol components as black carbon, brown carbon, absorbing and scattering mineral dust, etc. (Li et al., 2019).

This GRASP/Component approach derives fractions of aerosol components together with size distribution and non-spherical fraction of aerosol particle directly from the measured radiances without

an intermediate step of optical aerosol properties retrieval (Li et al., 2019). This is a significant methodological difference with other approaches for aerosol typing from satellite observations. For example, Russell et al., (2014) also demonstrated a possibility to identify aerosol type from POLDER-3 observations. However, that study analyzed aerosol optical properties derived from POLDER-3 by SRON algorithm using of aerosol classes/types (pure dust, polluted dust, biomass burning, urban/industrial, and marine aerosol) set of criteria formulated based on the AERONET retrievals (e.g., aerosol optical and microphysical parameters). In should be noted also, that GRASP/Component approach was applied to AERONET data and was demonstrated to derive valuable information about aerosol components , as well as to provide optical properties with the accuracy comparable to the standard AERONET retrievals (Li et al., 2019; Zhang et al., 2022).

Because the validation of aerosol optical properties (AOD, Ångström exponent (AE), AODF, coarse-mode AOD (AODC), aerosol absorption optical depth (AAOD), single-scattering albedo (SSA), etc.) generated by POLDER-3/GRASP-Component approach has been realized and discussed by Zhang et al. (2021), this study . This study presents the extensive analysis of aerosol composition products generated by GRASP/Component from full archive of the multi-angular polarimetric POLDER-3 observations. We present the climatological, global statistical analysis of satellite-retrieved aerosol absorbing components and scattering components with the assessment of consistency with general expectation to the extent possible. We also make comparisons of GRASP/Component BC and dust retrievals to those in MERRA-2 (Modern-Era Retrospective Analysis for Research and Applications, version 2) products. Our expectation, based on preliminary sparse analysis of derived aerosol component information (Li et al., 2019, 2020a, 2020b) and on the results of study by Zhang et al. (2021b) demonstrating component approach can provide comparable and sometime even better aerosol optical products, is that GRASP/Component approach generally can provide from POLDER like polarimetric data both conventional aerosol optical parameters and the parameters characterizing aerosol composition with sufficiently high accuracy.

2 Data and methodology description

2.1 POLDER-3 sensor

The PARASOL was launched on December 18, 2004 as a part of the A-Train constellation. POLDER-3, designed for the measurements of multispectral, multidirectional, and polarized radiances, onboard PARASOL satellite provides data for the period of March 2005 – October 2013 (Tanré et al., 2011). POLDER-3 has nine channels (440, 490, 565, 670, 763, 765, 865, 910, and 1020 nm) for the measurements of total radiance and three channels (490, 670, and 865 nm) for the measurements of polarization. The measurements are collected in up to 16 viewing angles per pixel with a resolution of 5.3 × 6.2 km^2 at nadir. In addition, it has been demonstrated that the multipolarization and multidirectional measurements of POLDER help to distinguish better cloudy and clear pixels (Buriez et al., 1997; Goloub et al., 1997; Parol et al., 1999; Zeng et al., 2011).

2.2 GRASP/Component product

We are discussing the advanced aerosol products obtained from POLDER-3 using GRASP algorithm. The efficiency and flexibility of GRASP ~~has~~ have been illustrated in many previous studies on applications to diverse remote sensing instruments, such as ground-based AERONET photometers and lidars (e.g., Benavent-Oltra et al., 2019; Lopatin et al., 2013, 2021; Titos et al., 2019; Tsekeri et al., 2017; Zhang et al., 2022, etc.), POLDER-3 (e.g., Chen et al., 2020; Dubovik et al., 2011; Li et al., 2019, 2020a, 2020b, etc.), DPC/GF-5 (Li et al., 2022), sky cameras (e.g., Román et al., 2017, 2021, etc.), polar-nephelometer data (e.g., Espinosa et al., 2017; Schuster et al., 2019, etc.). The papers by Dubovik et al. (2011, 2014, 2021a) presents the detailed description of the main concept of GRASP as well as the specific methodological introductions. In brief, GRASP employs the multi-term least square minimization (Dubovik, 2004; Dubovik et al., 2021a) for the implementation of statistically optimized fitting. The advantages of this concept have been initially demonstrated in the retrievals of the aerosol properties from ground-based AERONET sun/sky-radiometers (Dubovik et al., 2000, 2002a, 2002b, 2006; Dubovik and King, 2000). One of essential differences from traditional LUT algorithms is that GRASP performs online radiative transfer computations for multiple interactions of the scattered solar light in the atmosphere.

That is, GRASP searches the optimized fitting in the continuous space of solutions, whereas the traditional LUTs approaches search among the pre-computed solutions. This allows GRASP to explore a much larger parameter space (i.e., non-lognormal size distributions and orders of magnitude refractive indices) than tratidional approaches. The properties of surface reflectance in GRASP are modelled using Bidirectional Reflectance Distribution Function (BRDF) and Bidirectional Polarization Distribution Function (BPDF) models. Specifically, over land, the Ross-Li BRDF (Li and Strahler, 1992; Ross, 1981) and BPDF (Maignan et al., 2009) models are used considering geometrical and volumetric terms of the Ross-Li BRDF models nearly spectrally constant (Litvinov et al., 2011). The reflective properties of ocean surface are taken into account using Cox-Munk model (Cox and Munk, 1954) analogously to the many conventional approaches, the details are provided by Dubovik et al. (2011) and Frouin et al. (2019). The GRASP is open-source code that is provided together with a described documentation at GRASP-OPEN website https://www.grasp-open.com (last access: 30 November 2021).

Several different versions of aerosol optical products derived by previous GRASP (Optimized, High Precision, and Models) approaches for the full archive of POLDER-3 observations have been generated and released for open access (Dubovik et al., 2019; Chen et al., 2020). Here, we provide only a brief description of these three approaches and their main differences that are relevant to present analysis. As described in Dubovik et al. (2011), the solution vector in the all these three GRASP configurations can be written as Eq. (1):

$$\mathbf{a} = (\boldsymbol{a}_v, \boldsymbol{a}_n, \boldsymbol{a}_k, \boldsymbol{a}_{sph}, \boldsymbol{a}_{Vc}, \boldsymbol{a}_h, \boldsymbol{a}_{brdf1}, \boldsymbol{a}_{brdf2}, \boldsymbol{a}_{brdf3}, \boldsymbol{a}_{bpdf})^T, \tag{1}$$

where the elements representing the normalized logarithms of $dV(r)/dlnr$, real part of complex refractive index, imaginary part of complex refractive index, spherical particles fraction, total volume concentration, mean altitude of the aerosol layer, the parameters in BRDF and BPDF model are characterized by the vectors of $\boldsymbol{a}_v, \boldsymbol{a}_n, \boldsymbol{a}_k, \boldsymbol{a}_{sph}, \boldsymbol{a}_{Vc}, \boldsymbol{a}_h, \boldsymbol{a}_{brdf1}, \boldsymbol{a}_{brdf2}, \boldsymbol{a}_{brdf3}, \boldsymbol{a}_{bpdf}$, respectively. The GRASP aerosol optical products derived by Optimized, HP and Models approaches are generated and released publicly as daily, monthly, seasonal, yearly and climatological datasets in Level-2 and Level-3 (Chen et al., 2020). Level-2 represents the quality-filtered products with an initial resolution of satellite observations. There are two different spatial resolution of 0.1° and 1° for the Level-3 products. Level-3

245 ~~represents the products with a resolution of 0.1° and 1° grid box, respectively.~~ Hereafter all the GRASP/Component climatology is presented at 0.1° × 0.1° spatial resolution, except, the comparisons with MERRA-2 will be at 0.5° × 0.625° (that is, the GRASP/Component products are regridded into the same resolution of 0.5° × 0.625° as of MERRA-2). Level-0 represents the raw data and Level-1 represents daily files of retrievals considered as results of intermediate processing, which could be provided under

250 request.

As mentioned above, GRASP is a versatile algorithm, that can be applied to diverse observations and can be served as an assessable community tool for testing new and innovative ideas for interpretation of remote sensing measurements, e.g. using synergy of different observations (Dubovik et al., 2021a;

255 Lopatin et al., 2021). The most recent "GRASP/Component" approach described in the study of Li et al. (2019), can derive some size-resolved aerosol composition information attempting to discriminate the ~~contribution~~ contributions of such species as black carbon, brown carbon, coarse-mode absorbing (mainly representing iron oxides in mineral dust), fine- and coarse-mode non-absorbing soluble and insoluble, etc. Specifically, forward model of GRASP/Component uses the fixed refractive index for each component

260 (see Table S1) and based on the given component fractions calculates the complex refraction indices of aerosol mixture for simulating the observations. Correspondingly, the state vector in the GRASP/Component configuration includes the ~~component factions~~ fractions of components instead of refractive indices (Li et al., 2019):

$$\mathbf{a} = (\boldsymbol{a}_v, \boldsymbol{a}_{fract}, \boldsymbol{a}_{sph}, \boldsymbol{a}_{Vc}, \boldsymbol{a}_h, \boldsymbol{a}_{brdf1}, \boldsymbol{a}_{brdf2}, \boldsymbol{a}_{brdf3}, \boldsymbol{a}_{bpdf})^T,$$ (2)

265 where $\boldsymbol{a}_{fract}$ represents the aerosol component fractions.

Thus, the main conceptual difference of GRASP/Component from GRASP Optimized and High Precision is the retrieval of volume fractions of ~~6~~ six components (black carbon, brown carbon, fine- and coarse-mode non-absorbing insoluble, coarse-mode insoluble absorbing, mainly representing iron oxides in

270 mineral dust, and relative humidity for the host calculation) instead of direct retrieval of the real and imaginary parts of complex refractive index at each wavelength (12 parameters in GRASP Optimized and High Precision). ~~instead of the real and imaginary parts of complex refraction index retrieval for each~~

~~wavelength (12 parameters in GRASP Optimized and High Precision).~~ Thus, the number of unknowns is reduced in GRASP/Component compared to GRASP Optimized, High Precision. In addition, the spectral refractive index of each species assumed in the component model presents extra constraints on the spectral dependences of complex refraction index of aerosol mixture. The advantage in GRASP/Component associated with the reduction of unknowns and additional constraints on spectral dependences was discussed by the study of Zhang et al. (2021). In the contrast, the GRASP/Models approach retrieves even smaller number of parameters since it considers aerosol as an external mixture of aerosol components with a priori fixed all optical properties (particle size, refractive index and fraction of spheres). However, GRASP/Models ~~seem~~ seems to have some limitations in deriving such detailed parameters as AE, AODC, AODF, etc. (Chen et al., 2020).

The GRASP/Component approach assumes internal mixing of aerosol component for fine and coarse aerosol modes, which requires a mixing rule on the estimation of components for the aerosol mixture. Maxwell-Garnett (MG) effective medium approximation is employed in GRASP/Component, as one of main mixing rules, to estimate an effective refractive index of aerosol mixture considering several insoluble components presenting soluble host, such as ammonium nitrate (or sulphate) (Bohren and Huffman, 1983; Lesins et al., 2002). The hygroscopicity of ammonium nitrate has been quantitatively described in details (Tang, 1996), thus the proportions and properties of ammonium nitrate and aerosol water content are selected for calculation of optical properties of the host. Thus, using fractions of the components and relative humidity as variable parameters, the refractive index of a particle composed by several insoluble components (e.g., BC, BrC, mineral dust etc.) suspended in such host were determined by the MG equations based on the calculation of electric fields. First, the complex dielectric constant of each aerosol component is computed from the corresponding complex refractive index. Then, the Maxwell Garnett dielectric functions are used for calculating the dielectric constant of the aerosol mixture from component fractions and their dielectric constants. At last, the complex refractive index of aerosol mixture can be obtained from the complex dielectric constant of aerosol mixture.

Currently, the complete POLDER-3 data archive has been processed by GRASP/Component approach to provide extensive aerosol component concentration and aerosol optical properties retrievals. Similar to previous products described in Chen et al. (2020), extensive GRASP/Component products generated as daily, monthly, seasonal, yearly and climatological datasets in Level-2 and Level-3 are publicly assessable at GRASP-open (https://www.grasp-open.com/). Although several regional applications of this GRASP/Component have been discussed in several studies (Li et al., 2020a, 2020b; Zhang et al., 2021), the climatology of derived aerosol component distribution has not yet been fully analyzed in details and therefore the full potential of this new satellite derived aerosol composition was not fully clarified for the broad aerosol community. Therefore, the main focus of this study ~~the study in paper~~ is on the analysis/verifications of aerosol composition (fractions) retrievals and considering the apparent climatological patterns of aerosol composition. ~~the apparent of aerosol composition climatological patterns.~~ Indeed, Zhang et al. (2021) validated GRASP/Component optical properties against AERONET data and concluded that generated total AOD values have minimal bias both over land (-0.02 for 550 nm) and ocean (0.01 for 550 nm), similar to total AOD provided by GRASP/Models, while the detailed properties such as AE, AODF and AODC have similarly good validation metric as GRASP/HP. ~~This suggested that GRASP/Component provided~~ This suggests that the GRASP/Component products provide the overall most consistent both total and detailed aerosol properties (e.g., spectral AODF, AODC, and SSA etc.) with respect to previous GRASP (Models, HP, and Optimized) products.

2.3 MERRA-2 data

MERRA-2 is the new version of atmospheric reanalysis publicly distributed by the NASA Global Modeling and Assimilation Office (Gelaro et al., 2017; Randles et al., 2017) and the detailed description can be found in (Buchard et al., 2017; Gelaro et al., 2017; Randles et al., 2017). The AOD products derived from the ground-based AERONET measurements and satellite observations (e.g., MODIS, MISR) are assimilated into the MERRA-2 by the GEOS-5 (Goddard Earth Observing System). The GOCART (Goddard Chemistry, Aerosol, Radiation and Transport) model is employed for the simulation of aerosol compositions such as black carbon, organic carbon, dust, etc. Up to now, numerous studies presented quantificational validations and assessments of different MERRA-2 products on a global or regional scale

using measurements, such as AOD (Randles et al., 2017; Song et al., 2018; Sun et al., 2019), PM2.5 (Buchard et al., 2016; Song et al., 2018), and surface BC concentration using measurements at several separate sites in China (Qin et al., 2019; Xu et al., 2020). However, MERRA-2 BC and dust column 330 ~~columnar~~ concentration products have not been compared to any observations globally. In this study, we employ the monthly MERRA-2 BC and dust column ~~columnar~~ concentration products in a spatial resolution of 0.5° × 0.625° as available from the NASA website (https://daac.gsfc.nasa.gov).

3 Global POLDER-3 GRASP/Component aerosol products

The POLDER-3 GRASP/Component retrieval provides following parameters characterizing the aerosol 335 composition: volume fractions of Black Carbon, Brown Carbon, fine/coarse mode non-absorbing soluble and insoluble, coarse mode absorbing, as well as fine/coarse mode aerosol water content. From the view point of optical properties, the strongly absorbing and mostly scattering aerosol components are convenient to analyse separately.

3.1 GRASP/POLDER-3 absorbing component products

The following aerosol components determine the aerosol absorption: BC and BrC in fine mode particles and coarse mode absorbing insoluble (CAI) component mainly representing iron oxides element contained in mineral dust.

3.1.1 Black Carbon (BC)

345 Figure 1 presents the distribution of seasonal BC column ~~columnar~~ mass concentration in the climatological products derived by the GRASP/Component from POLDER-3 observations and Figure 2 shows the corresponding standard deviations (STD, calculated from all months data during the period 2005－2013, same for other components in the following) divided by the mean of BC concentration. These satellite-derived BC concentrations present a noticeable temporal and spatial variations that are 350 consistent with the distribution of biomass burning events. For example, over the African continent, the

high BC concentrations can be observed over the Sahel region during the DJF season extending to southern Africa region during the JJA and SON seasons as intense agricultural burnings occurring in the sub-Sahelian region of Africa and progressing from north to south following the African monsoon cycle. In addition, large STD/Mean values are obtained for BC concentrations over southern Africa region during the SON season. The elevated BC concentrations are also retrieved over South America during the entire biomass burning season (from August to November, see Fig. 1), which is in line with the previous studies (Koren et al., 2007; Lei et al., 2021). At the same time, high STD/Mean values for BC concentration are obtained during the SON season over the South America, which indicates the large interannual variability. Natural factors such as weather and cultural practices are known to make important contributions to the significant interannual variability of biomass burning in the Amazon basin rainforest (Koren et al., 2007). Fig. 2 also indicates high STD/Mean values for BC concentration in Asia during the MAM season, which is associated with large interannual variability of fires in the biomass burning season (such as over Indo-China Peninsula). ~~Fig. 2 also indicates that low STD/Mean values for BC concentration in Asia, Europe and North America are observed when the intensity of anthropogenic emissions is small.~~ Yearly means of BC column ~~columnar~~ mass concentration for the period from March 2005 to October 2013 is presented in Fig. 3. We should point out that many BC particles are generated from anthropogenic activities such as in China and India (shown in Fig. 4), however, our global climatology also indicates that the BC concentration emitted from biomass burning in Africa and South America produces much higher BC concentrations than the anthropogenic emissions, e.g., in China and India (see Fig. 1 and 3). The climatology of the BC mass concentrations over East and South Asia regions are studied in detail by Li et al. (2020b), which demonstrated that GRASP/Component retrievals can characterize well the temporal and spatial variations of light-absorbing carbon (BC and BrC) in East and South Asia. A reasonable agreement between in situ ground-measured and satellite-derived BC mass concentration in China has been early demonstrated by Li et al. (2020b). For instance, the BC product of GRASP/Component and the in situ measurements agrees with the mean absolute difference of about 2.7 $\mu m/m^3$, ranging from 0.09 $\mu m/m^3$ to 7.8 $\mu m/m^3$ and the relative difference of about 40%, ranging from 2.6% to 60%, respectively (Li et al., 2020b). High BC proportions in Asia are found to be associated strongly with biomass burning events (such as agriculture waste open burning event during MAM over

the Indo-China Peninsula or JJA in the North China Plain) and fossil fuel combustion (Li et al., 2020b).

380 It is noted that high BC concentration in India and China during the DJF season is strongly associated with anthropogenic activity (e.g., Li et al., 2019). The interpretation of some BC concentration over ocean, especially in high latitude near the polar region, should be taken with more caution because the sensitivity to the absorption and thus to the BC signal is limited when the aerosol loadings are very low and the retrievals are more uncertain, which is the same situation for large STD/Mean values when BC

385 concentration is very low. In this respect it can be noted that based on the sensitivity tests and uncertainty assessments in the study of Li et al. (2019), the uncertainty in BC fraction is within 50% when AOD (440 nm) is larger than 0.4 and fraction is higher than 0.01. This BC uncertainty is mainly resulting from the reported in the literature highly variable complex refractive index of BC, e.g., from 1.75 + 0.63i to 1.95 + 0.79i (Bond et al., 2013; Bond and Bergstrom, 2006). Similarly, the uncertainty in BC retrievals from

390 ground-based AERONET measurements is about 50% (Schuster et al., 2016b).
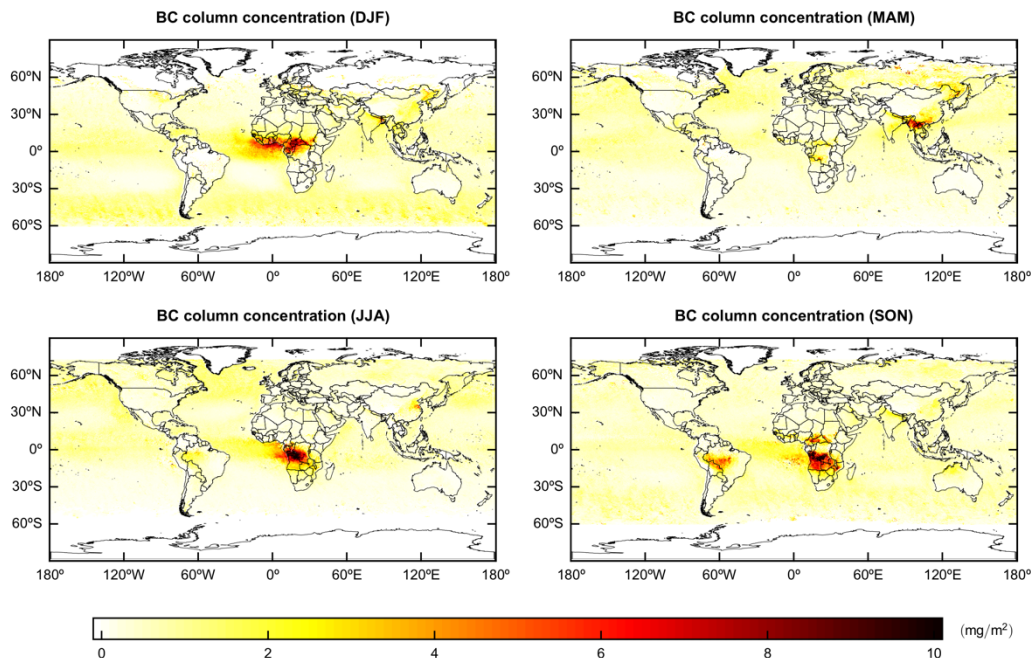
Figure 1: Spatial distribution of seasonal BC ~~columnar~~ column mass concentration (mg/m^2) derived by the GRASP/Component approach from POLDER-3 observations. DJF: December-January-February; MAM: March-April-May; JJA: June-July-August; SON: September-October-November.
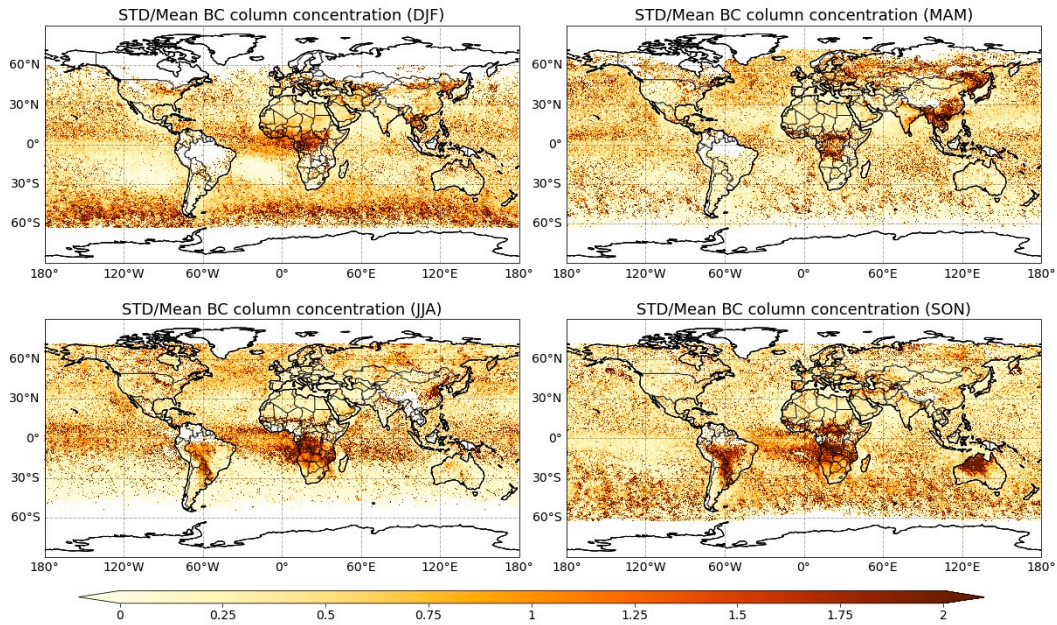
Figure 2: The standard deviation (STD)/Mean for seasonal BC ~~columnar~~ column mass concentration in Fig. 1 derived by the GRASP/Component approach from POLDER-3 observations. DJF: December-January-February; MAM: March-April-May; JJA: June-July-August; SON: September-October-November.
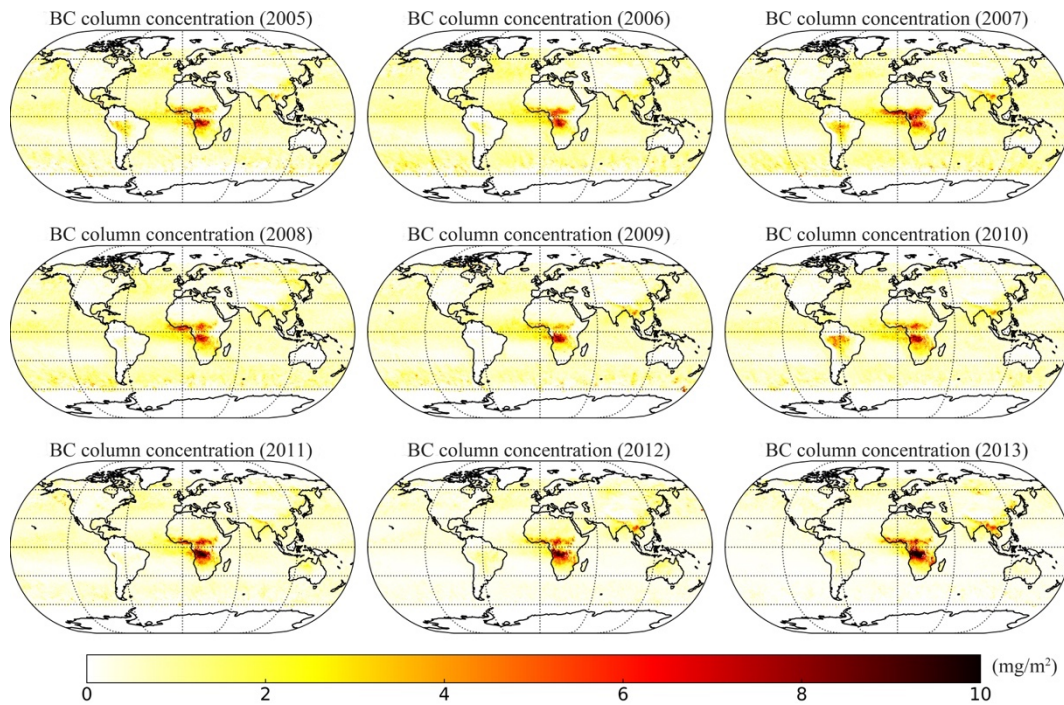
405

Figure 3: Yearly mean of BC ~~columnar~~ column mass concentration (mg/m^2) ~~in resolution of~~ derived by GRASP/Component approach from POLDER-3 observations for the period from March 2005 to October 2013.
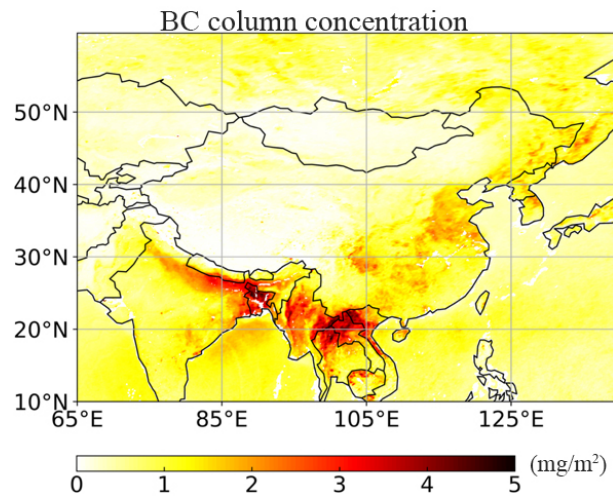
Figure 4: Climatological BC ~~columnar~~ column mass concentration (mg/m^2) derived by the GRASP/Component approach from POLDER-3 observations for the period from March 2005 to October 2013 in Asia.

3.1.2 Brown Carbon (BrC)

Unlike strong and spectrally flat absorption of BC component, BrC shows a strong spectral dependence of absorption that decreases from shorter to longer wavelengths and a weaker absorption than BC (Chakrabarty et al., 2010; Kirchstetter et al., 2004; Wonaschütz et al., 2009). Fig. 5 and 6 present the satellite-derived seasonal BrC ~~columnar~~ column mass concentration issued by GRASP/Component for the period 2005－2013 and the corresponding standard deviations (STD) divided by the mean of BrC concentration, respectively. The seasonal variation and spatial distribution of BrC ~~columnar~~ column mass concentration show similarities to the BC pattern (in Fig. 1) as these light-absorbing carbonaceous particles are generally emitted from same emission sources such as biomass or fossil fuel combustion. Therefore, high BrC concentration are also observed over Africa, South America and the Indo-China Peninsula in Asia during the corresponding biomass burning period as discussed above for the BC concentration. High BrC concentration observed over the ocean near the continent is rather associated with the aerosol transport. For example, strong fires occurring from north to south Africa during the whole biomass burning period make large contributions to the BrC particles burden over the Atlantic Ocean near the African continent during the DJF, JJA, and SON seasons. Elevated BrC concentrations are also seen over the Pacific Ocean during the MAM season that can be transport of biomass burning emissions from the Indo-China Peninsula (Li et al., 2020b). The observed in the global inter-annual climatology (Fig. 1 and Fig. 5) seasonal variabilities of BC and BrC concentrations in Asia were already analysed in the earlier study by Li et al. (2020b). Although statistically significant differences of smoke properties have been observed for fires in different fuel types such as forests, savannas, and grasslands (Noyes et al., 2021), our component retrievals indicate that the elevated BC concentrations in this work were attributed to fresh biomass burning aerosols while those of the BrC to the aged biomass burning aerosols. Indeed, interactions with atmospheric gases (e.g., O_3, NO_2, and SO_2) together with higher atmospheric water

content over ocean can change the morphology and optical property of BC particles by oxidization and coating, e.g., (Adachi and Buseck, 2013; China et al., 2013; Decesari et al., 2002; Zhang et al., 2008). Therefore, the meteorological factors and the atmospheric gases variability are also expected to contribute

440   to the BrC seasonal and interannual variability. It can be seen from Fig. 6 that STD/Mean values present no significant differences, which is same to the small interannual variability of BrC concentration in Fig. 7 except over the southern Africa during the SON season (low concentration in 2012 and 2013). For the proper data interpretation, it is worth noting that the uncertainty in BrC fraction is normally less than 50% if the BrC fraction is above 0.1, even for very low AOD (smaller than 0.05), although the uncertainty is

445   large in the case of small BrC fraction and low aerosol loading; the error estimations for GRASP/Component were conducted in (Li et al., 2019).
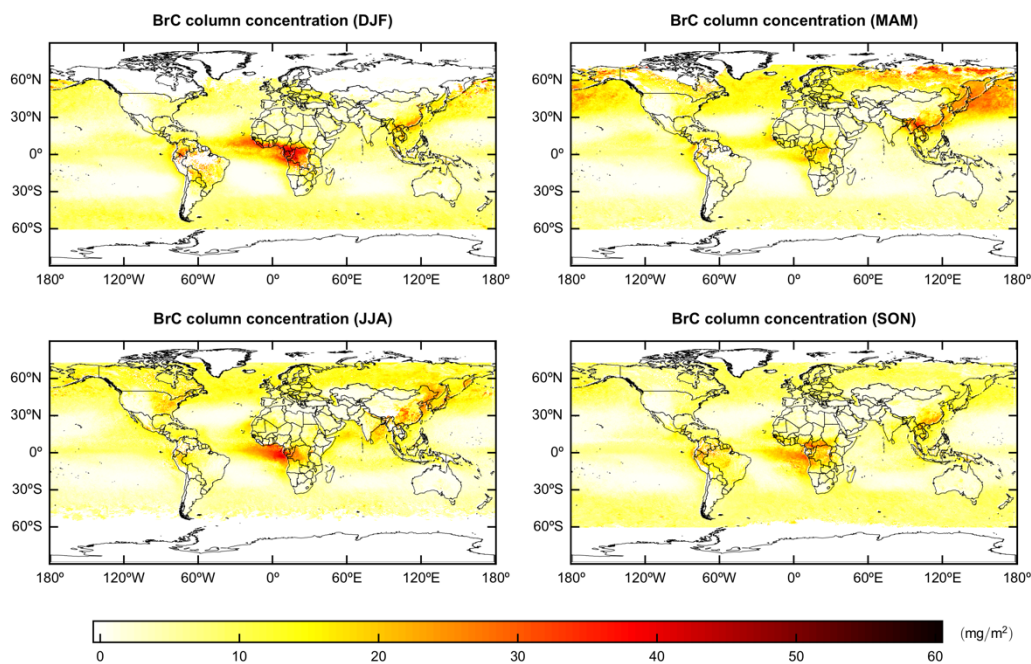
Figure 5: Spatial distribution of seasonal BrC ~~columnar~~ column mass concentration (mg/m²) derived by the GRASP/Component approach from POLDER-3 observations. DJF: December-January-February;

450   MAM: March-April-May; JJA: June-July-August; SON: September-October-November.
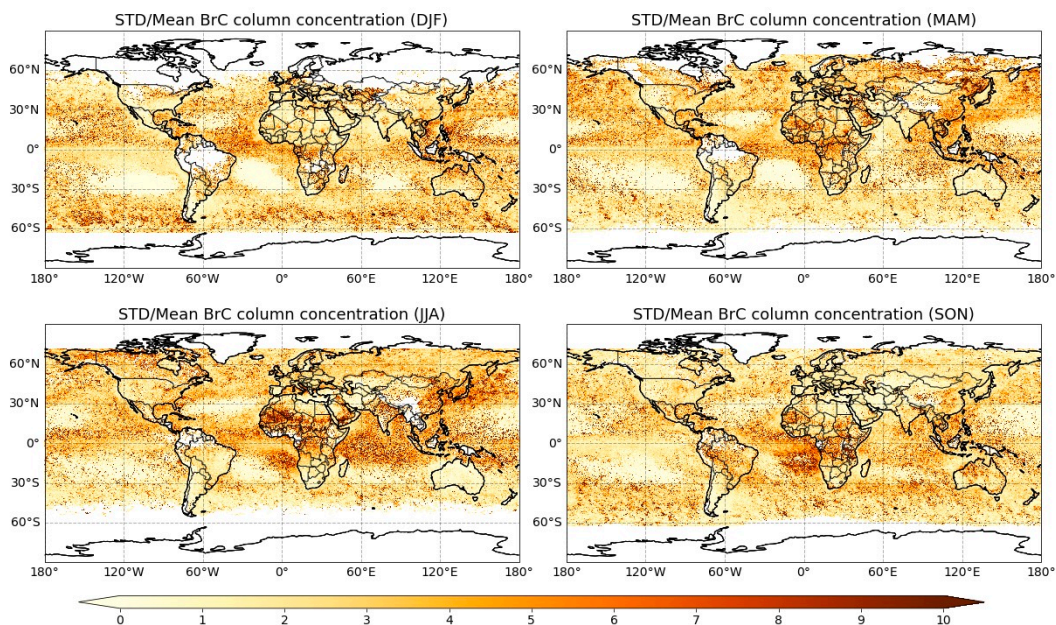
455 **Figure 6:** The standard deviation (STD)/Mean for seasonal BrC ~~columnar~~ column mass concentration in Fig. 5 derived by the GRASP/Component approach from POLDER-3 observations. DJF: December-January-February; MAM: March-April-May; JJA: June-July-August; SON: September-October-November.

460
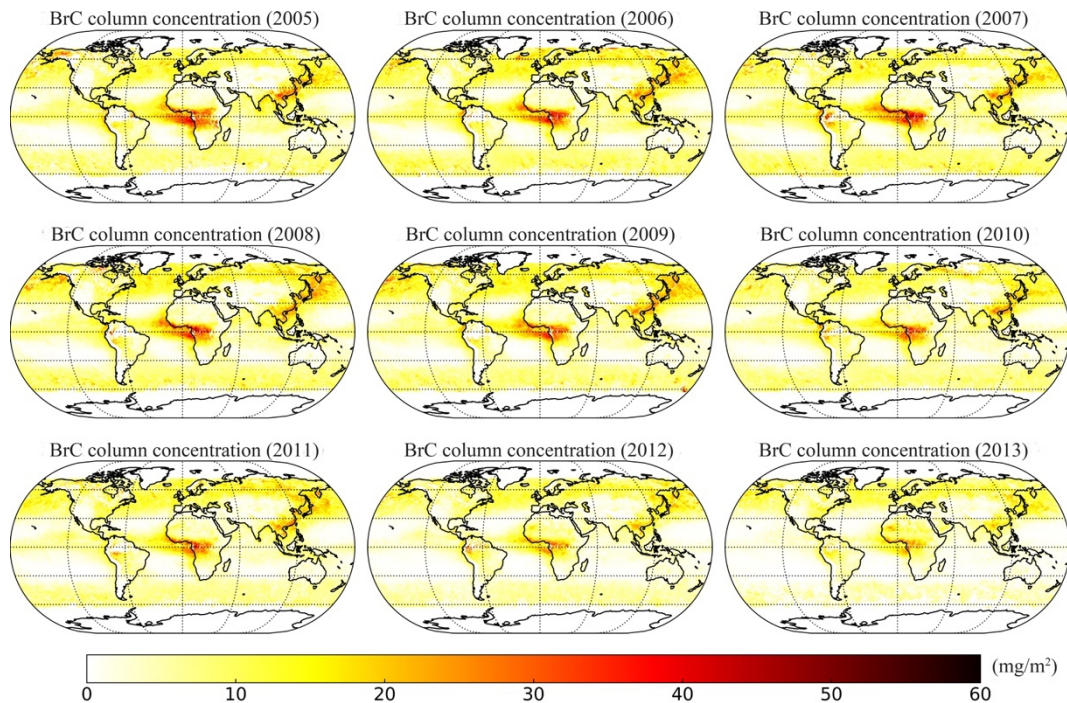
Figure 7: Yearly mean of BrC ~~columnar~~ column mass concentration (mg/m²) derived by the
GRASP/Component approach from POLDER-3 observations for the period from March 2005 to October
2013.

3.1.3 Coarse mode Absorbing Insoluble (CAI) aerosol component

Due to the absorption of hematite and goethite (free iron) contained in dust particles, mineral dust also
indicates a spectral absorbing signature that stronger absorption at short wavelength and weaker
absorption at long wavelength. In order to know the global distribution of free iron concentration for its
important biogeochemical and radiative impacts, coarse mode absorbing insoluble (CAI) component was
identified as an important species in the GRASP/Component approach (Li et al., 2019). At the same time,
because of a similar tendency in spectral absorption for BrC and CAI, the size-resolved component
configuration that light-absorbing carbonaceous components (BC and BrC) are assumed to be absorbing
component in the fine mode aerosol particles and CAI mainly representing iron oxides is assumed to be
absorbing component in the coarse mode aerosol particles was selected (Li et al., 2019). Fig. 8 shows the

satellite-derived seasonal CAI ~~columnar~~ column mass concentration in the climatological products by the GRASP/Component for the period 2005 − 2013. As discussed by Li et al. (2019), CAI particles mainly

480 represent iron oxides element contained in mineral dust. From Fig. 8, we can see that elevated CAI concentration are observed over the Sahara in western Africa, the Taklimakan in northwest China and over the Arabian Peninsula during the MAM and JJA seasons, which locations represent the global dust belt. Interesting to note that very low CAI aerosol concentrations are obtained over the Bodélé Depression, which indicates highly scattering dust particles (see the hot spot in Figs. 11 and 14 during the DJF season).

485 This fact is consistent with the known dust composition nature of the Bodélé containing the dolomites mainly (Formenti et al., 2011). The maximum mass ratio of absorbing dust to scattering dust in our retrievals was found of about 5%, which is consistent with the known mass fraction of iron oxides varying from 3% to 5% in the desert dust measurements (Guieu et al., 2002; Zhang et al., 2003). ~~It should be mentioned here however that our retrievals are constrained by the maximum value of iron oxides volume~~

490 ~~fraction of 3%. At the same time, this maximum value is practically never achieved indicating that the optical signal can be explained by iron oxides mass fraction within 5% (as the density is 4.8 g/cm³ for iron oxides and 2.5 g/cm³ for scattering dust component).~~ The characteristics presented in the climatological CAI distribution (Fig. 8) are also consistent with the results of previous studies (Formenti et al., 2008; Krueger et al., 2004; Lázaro et al., 2008) reporting large proportions of iron oxides in dust

495 originated from the Sahel belt between 0 and 20° N and Saudi Arabia, but low iron oxides content in the Chad Basin. The STD/Mean of seasonal CAI ~~columnar~~ column mass concentration (Fig. 9) generally show high values in the desert dust regions that are mostly due to the significant changes in 2012 and 2013 shown by yearly means of CAI (Fig. 10).

500 It should be recalled that the CAI particles are parameterized in the GRASP/Component approach as particles having spectral absorption of iron oxides and this is the only the absorbing specie assumed in the coarse mode due to the limitations of measurements sensitivity. However, other light-absorbing species presenting in coarse-mode can produce similar signal and be erroneously interpreted as iron oxides. For instance, it can be noted that the CAI particles appear also in the regions and seasons

505 associated with biomass burning, such as in South America during the SON season when strong biomass

burning events occur. The CAI in this case is therefore an indicator that carbonaceous particles might be appearing in coarse mode by some mechanisms. Alternatively, some CAI particles appearing in South America may be originating in dust transport from western Africa. This is in line with the previous studies reporting the African dust transport over the Atlantic Ocean, Caribbean, Central America, and South America (during the DJF and MAM seasons) (Griffin et al., 2002; Kalashnikova and Kahn, 2008; Prospero and Lamb, 2003; Prospero and Mayol-Bracero, 2013). Analogously, some CAI particles observed in northern and eastern China during the MAM season are transported from strong dust emission sources in the Taklimakan desert. Based on the results of Li et al. (2019), the uncertainty in CAI fraction associated with employed refractive index is within 50% excluding the case of very low CAI fraction, below 0.005. Thus, the CAI concentrations are expected to have large uncertainties over ocean and in high latitude near the polar region (such as the ocean around 60° S) where also the AOD is generally very low. Also, cloud contaminations that are more probable in those high latitude areas can be misinterpreted as apparent dust like aerosols.
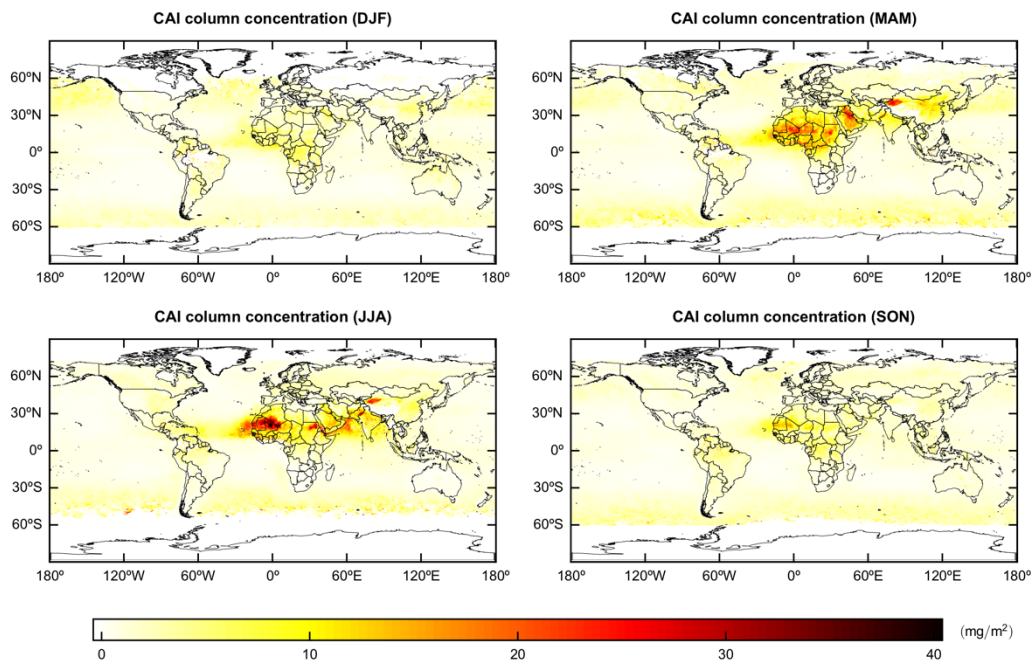
Figure 8: Spatial distribution of seasonal CAI (Coarse mode Absorbing Insoluble) ~~columnar~~ column mass concentration (mg/m^2) derived by the GRASP/Component approach from POLDER-3 observations. DJF: December-January-February; MAM: March-April-May; JJA: June-July-August; SON: September-October-November.
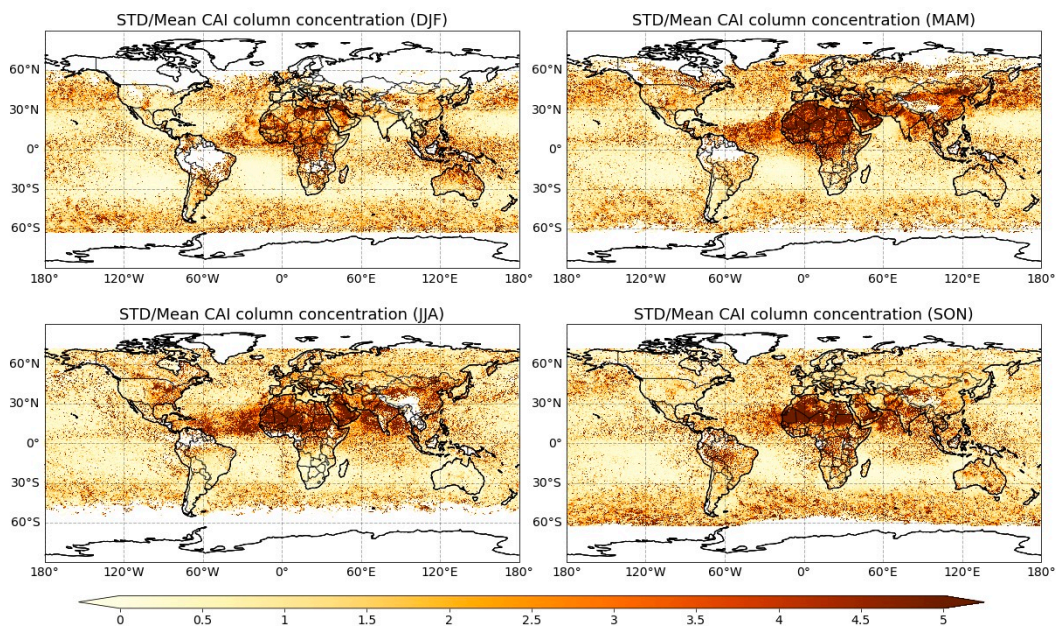
Figure 9: The standard deviation (STD)/Mean for seasonal CAI ~~columnar~~ column mass concentration in Fig. 8 derived by the GRASP/Component approach from POLDER-3 observations. DJF: December-January-February; MAM: March-April-May; JJA: June-July-August; SON: September-October-November.
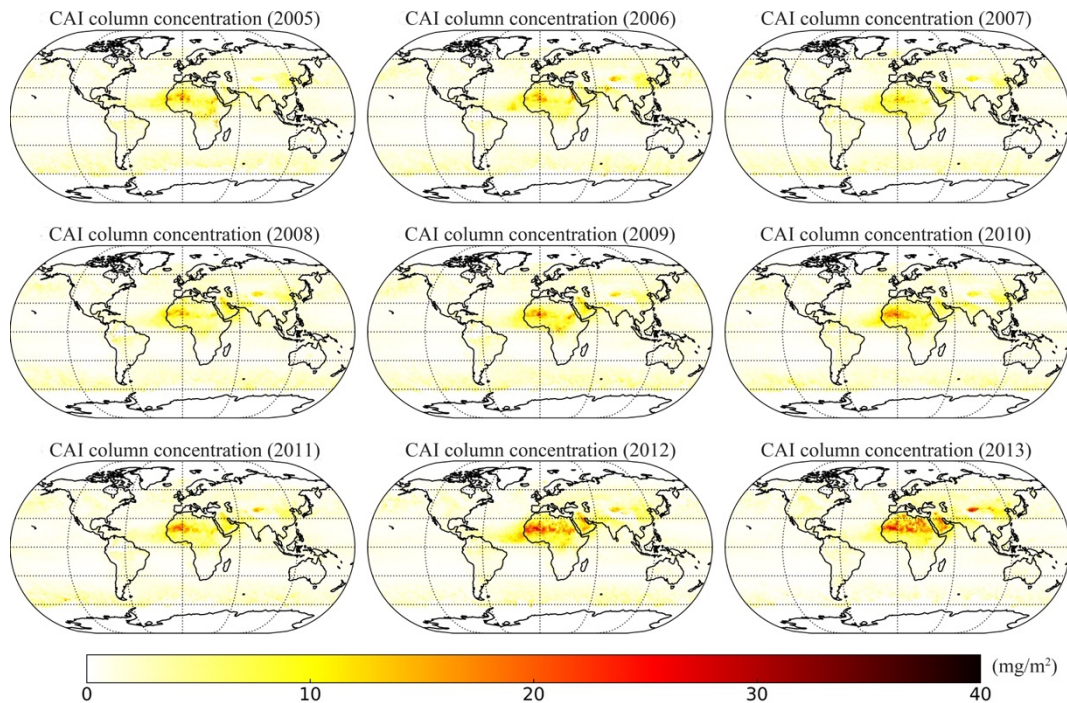
535

Figure 10: Yearly mean of CAI ~~columnar~~ column mass concentration (mg/m²) ~~in a resolution of~~ derived by the GRASP/Component ~~algorithm from~~ approach from POLDER-3 observations for the period from March 2005 to October 2013.

540   3.2 GRASP/POLDER-3 scattering component products

As defined in Li et al. (2019), the weakly absorbing, mostly scattering aerosol components including coarse-mode non-absorbing insoluble component (CNAI), fine-mode non-absorbing insoluble component (FNAI), as well as Non-Absorbing Soluble (NAS) and Aerosol Water Content (AWC) in fine and coarse mode are discussed below.

545   3.2.1 Coarse-mode Non-Absorbing Insoluble (CNAI)

The distribution of seasonal coarse-mode non-absorbing insoluble (CNAI) aerosol component and the associated STD/Mean are presented in Fig. 11 and 12, respectively. Yearly means of CNAI ~~columnar~~ column mass concentration for the period from March 2005 to October 2013 is presented in Fig. 13.

Generally, the CNAI component represents the non-absorbing part of mineral dust particles. Fig. 11 and 13 reveal in details the global dust belt with noticeable maximum concentrations during the MAM and JJA seasons. The high STD/Mean values obtained over the main desert dust regions represent large interannual variability (Figs. 12 and 13). Specifically, the maximum CNAI concentration in the northern Africa shows a shift from lower to higher latitudes during the MAM and JJA seasons, which is associated with the change of the intertropical convergence zone. The most active dust emission source, Bodélé Depression, is seen well in the CNAI retrievals (shown in Fig. 11) with the peaks during the DJF and MAM seasons, consistent with studies of Todd et al. (2007) and Washington et al. (2003). High coarse-mode non-absorbing dust concentrations are observed over the Arabian Peninsula and Taklamakan in China during the MAM and JJA seasons while significant decrease appears during the SON and DJF seasons. In addition, a key dust emission source in southwest Asia, named Sistan region (Goudie, 2014; Léon and Legrand, 2003; Middleton, 1986), can be seen in Fig. 11 during the JJA season.

The well-known locations of source regions of mineral dust over the globe are reported by numerous studies: the Sahara region in the northern Africa (e.g., Choobari et al., 2014; Prospero et al., 2002); the Middle East and Arabian Peninsula (Ginoux et al., 2012; Prospero et al., 2002); the Sistan Basin (representing the region of Iran, Pakistan, Afghanistan); the desert regions in southwestern Asia (Alizadeh-Choobari et al., 2014; Kaskaoutis et al., 2015); the Taklamakan in China and Gobi (northern China–southern Mongolia) deserts (Ginoux et al., 2012); as well as several desert regions in central Asia (Elguindi et al., 2016) and in North America (Ginoux et al., 2012). All of them represent the Northern Hemisphere as location of the most important natural dust emission sources. Till present, the studies of these dust sources were conducted based on satellite remote sensing mostly providing the total AOD, coarse mode AOD or AOD related, under extra assumptions, to desert Dust Optical Depth (DOD) (Logothetis et al., 2021). Those studies were conducted based on derived dust indices, AOD, aerosol profiles and on thermal infrared signal, i.e. from products of Total Ozone Mapping Spectrometer (TOMS, Ginoux et al., 2012; Prospero et al., 2002), MODIS (Gui et al., 2021c; Remer et al., 2008; Schepanski et al., 2012; Song et al., 2021; Voss and Evan, 2020; Yu et al., 2019), Infrared Atmospheric Sounding Interferometer (IASI, Clarisse et al., 2019; Yu et al., 2019), MISR (Gui et al., 2021a; Kahn and Gaitley,

2015; Yu et al., 2019), Cloud–Aerosol Lidar with Orthogonal Polarization (CALIOP, Gui et al., 2021b, 2021c; Shikwambana and Sivakumar, 2018; Song et al., 2021). In this regard, the GRASP/Component product from POLDER-3 privies certainly more direct quantitative evaluation of the mineral dust

580   composition and its iron oxide content enabling studies of the trends and variability. For example, as presented in Fig. 13, over the Arabian Peninsula, the lower CNAI concentrations are obtained for 2005 – 2007 and higher values CNAI concentrations are obtained for 2008 – 2013 periods, which agrees well with the results of Notaro et al. (2015) indicating an inactive and active dust periods (1998 – 2005 and 2007 – 2013, respectively) over the Arabian Peninsula related to the sustained drought near the Fertile

585   Crescent region. MODIS DOD products indicated that the dust loadings have an increase over the Sahara region during the period 2003 – 2018 (Voss and Evan, 2020), which can be seen now quantitatively in Fig. 13. We should also point out that some CNAI particles observed near central-south Africa might be attributed to the coarse-mode non-absorbing insoluble organic particles that probably exist when and where there are strong carbonaceous aerosol emissions during the biomass burning events (in Fig. 13).
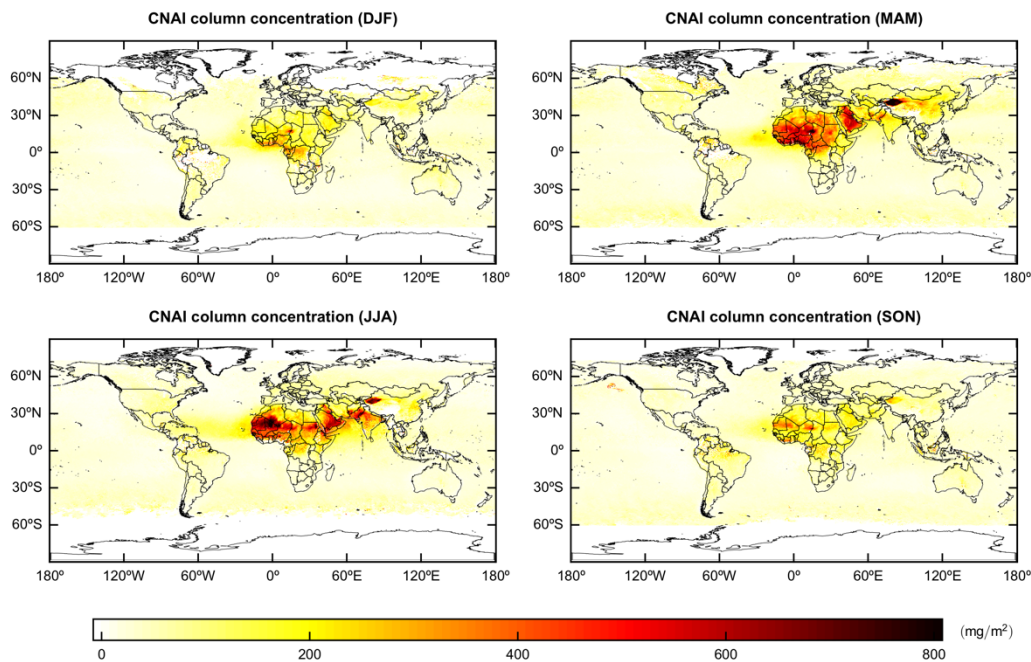
590

Figure 11: Spatial distribution of seasonal CNAI (Coarse-mode Non-Absorbing Insoluble component) ~~columnar~~ column mass concentration (mg/m²) derived by the GRASP/Component approach from POLDER-3 observations. DJF: December-January-February; MAM: March-April-May; JJA: June-July-August; SON: September-October-November.

595
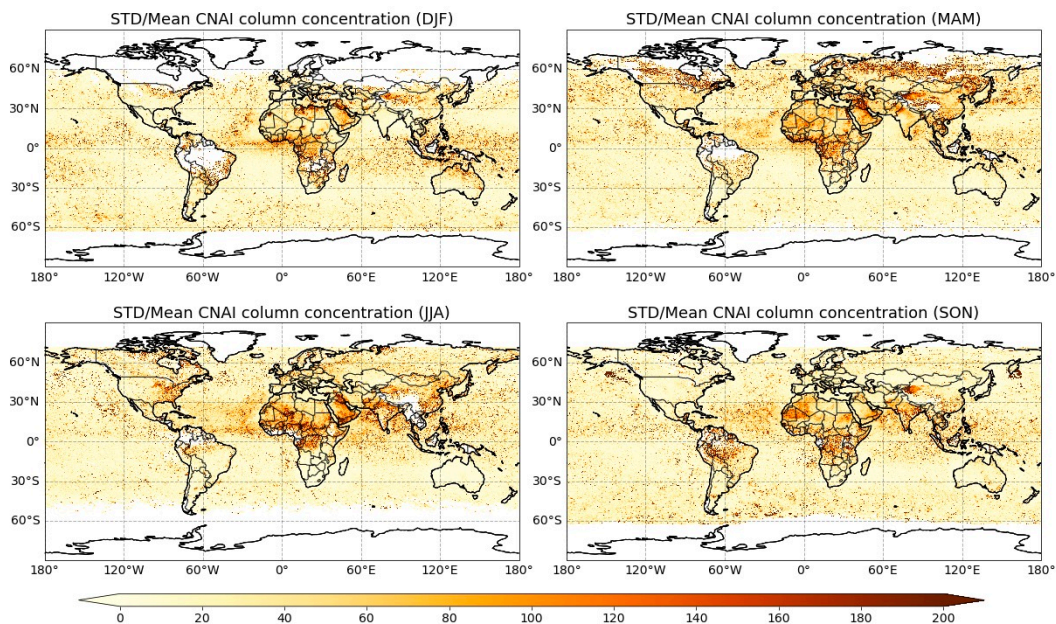
Figure 12: The standard deviation (STD)/Mean for seasonal CNAI ~~columnar~~ column mass concentration in Fig. 11 derived by the GRASP/Component approach from POLDER-3 observations. DJF: December-January-February; MAM: March-April-May; JJA: June-July-August; SON: September-October-November.

605
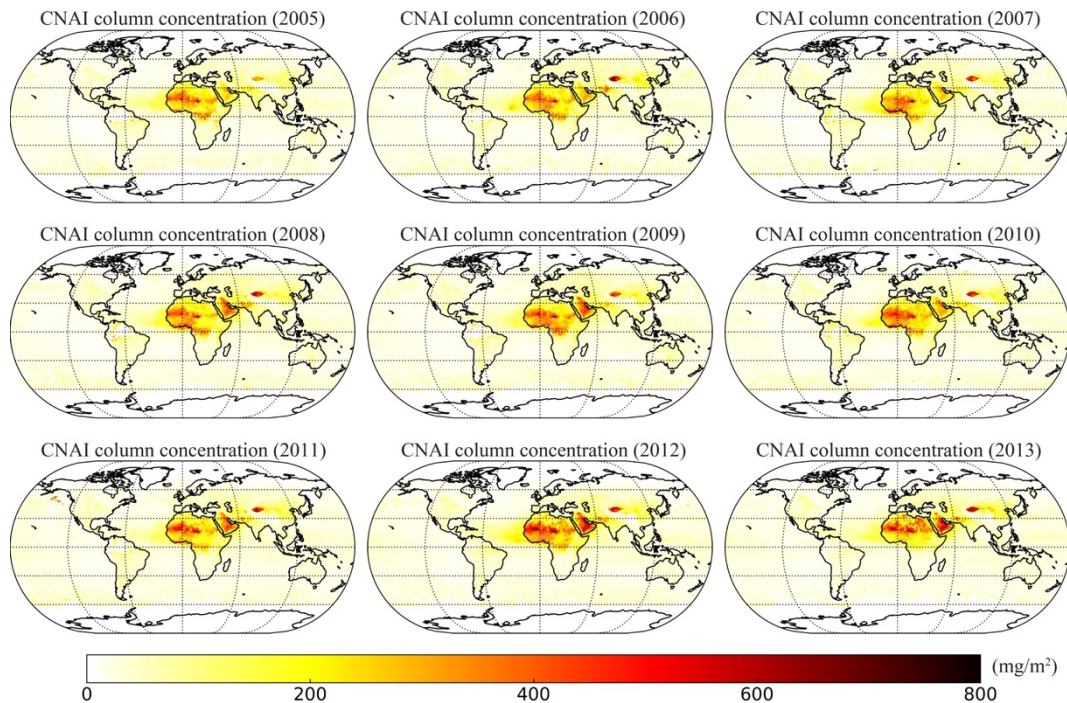
Figure 13: Yearly mean of CNAI ~~columnar~~ column mass concentration (mg/m^2) ~~in a resolution of 0.1°~~ ~~× 0.1°~~ derived by the GRASP/Component approach from POLDER-3 observations for the period from March 2005 to October 2013.

3.2.2 Fine-mode Non-Absorbing Insoluble (FNAI)

Figure 14 shows the pattern of seasonal fine-mode non-absorbing insoluble component (FNAI) ~~columnar~~ column mass concentration in the derived climatology, as well as the STD divided by the mean of FNAI concentration in Fig. 15. As aforementioned and discussed by Li et al. (2019), both scattering organic carbon and non-absorbing dust particles in fine-mode aerosol are labelled as FNAI in current GRASP/Component. Thus, significant similarities and differences are obviously seen between FNAI (Fig. 14) and CNAI (Fig. 8) spatio-temporal distributions. Specifically, similar CNAI and CAI, the spatio-temporal characteristics of global dust belt appears in the FNAI. That is, the concentrations appear over northern Africa, Bodélé Depression, Arabian Peninsula, and the Taklimakan Desert. However, the

differences are manifested in well-known for the biomass burning regions and seasons, i.e. in southern Africa and South America during the JJA and SON seasons, in the Indo-China Peninsula during the MAM season, as well as fossil fuel burning associated with strong anthropogenic activities in China and India. The retrieved FNAI particles, mainly representing the fine-mode scattering organic carbon, present good spatio-temporal consistency with the results of previous studies on the variability of anthropogenic and biomass burning emissions (Duncan et al., 2003; Zhang et al., 2008b, 2012). Large STD/Mean values are obtained over southern Africa and South America which can be attributed to the interannual variations of biomass burning events. For example, the yearly means of FNAI columnar column mass concentration shown in Fig. 16 presents extremely high FNAI concentration over South America in 2005, 2007, and 2010, which could be caused by the areas and frequency of El Niño-induced droughts and fires in this region. The uncertainty of the FNAI retrievals depends on the aerosol loading and is generally be less than 100%.
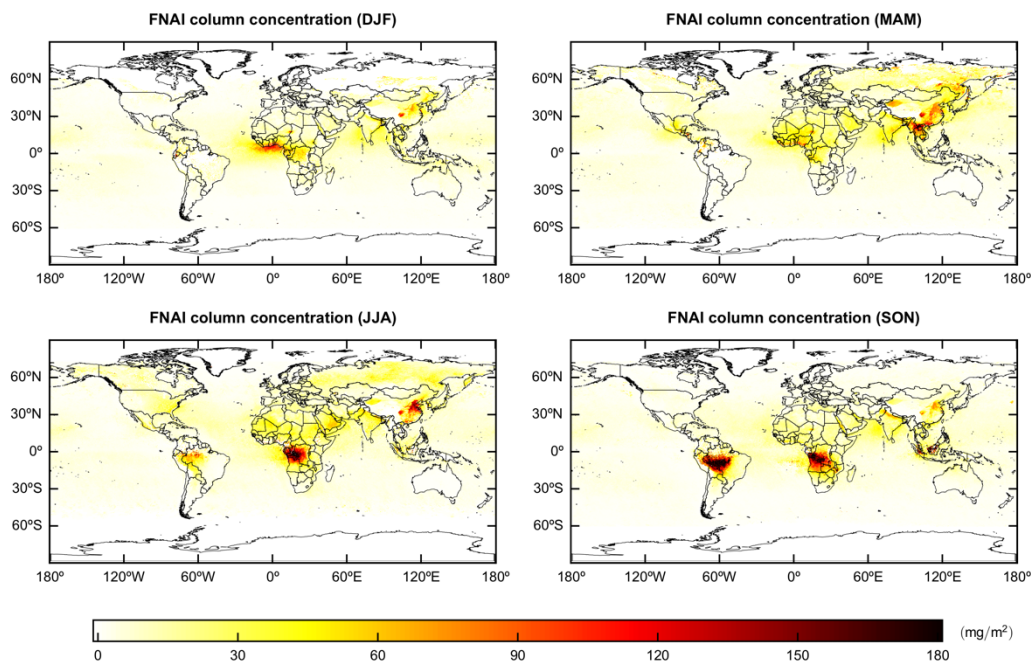
Figure 14: Spatial distribution of 0.1° × 0.1° seasonal FNAI (Fine mode Non-Absorbing Insoluble component) columnar column mass concentration (mg/m^2) derived by the GRASP/Component approach

from POLDER-3 observations. DJF: December-January-February; MAM: March-April-May; JJA: June-July-August; SON: September-October-November.
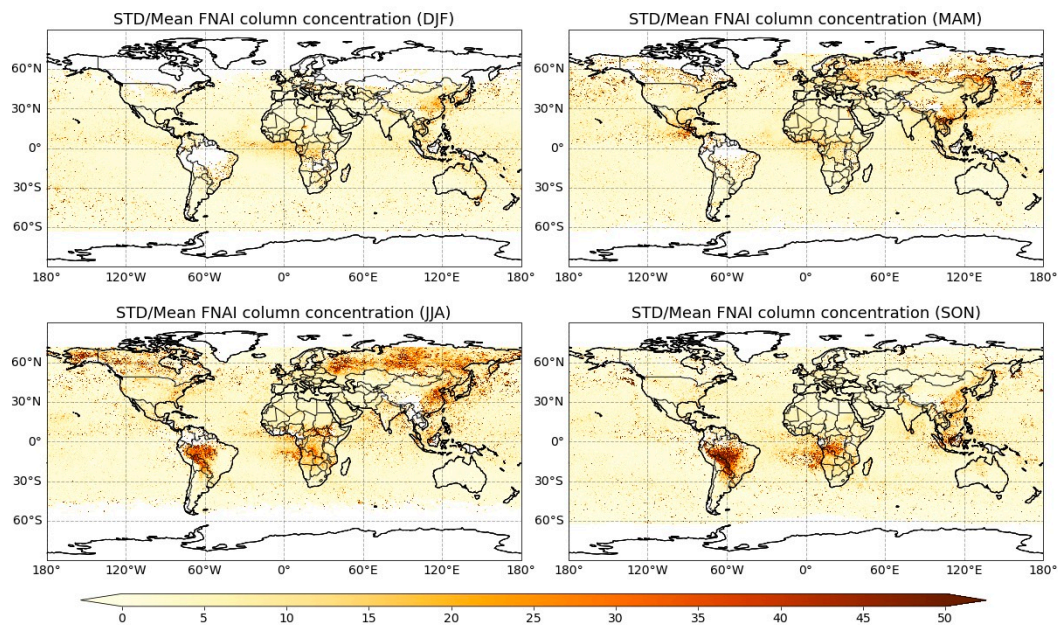
640

Figure 15: The standard deviation (STD)/Mean for seasonal FNAI ~~columnar~~ column mass concentration in Fig. 14 derived by the GRASP/Component approach from POLDER-3 observations. DJF: December-January-February; MAM: March-April-May; JJA: June-July-August; SON: September-October-November.

645
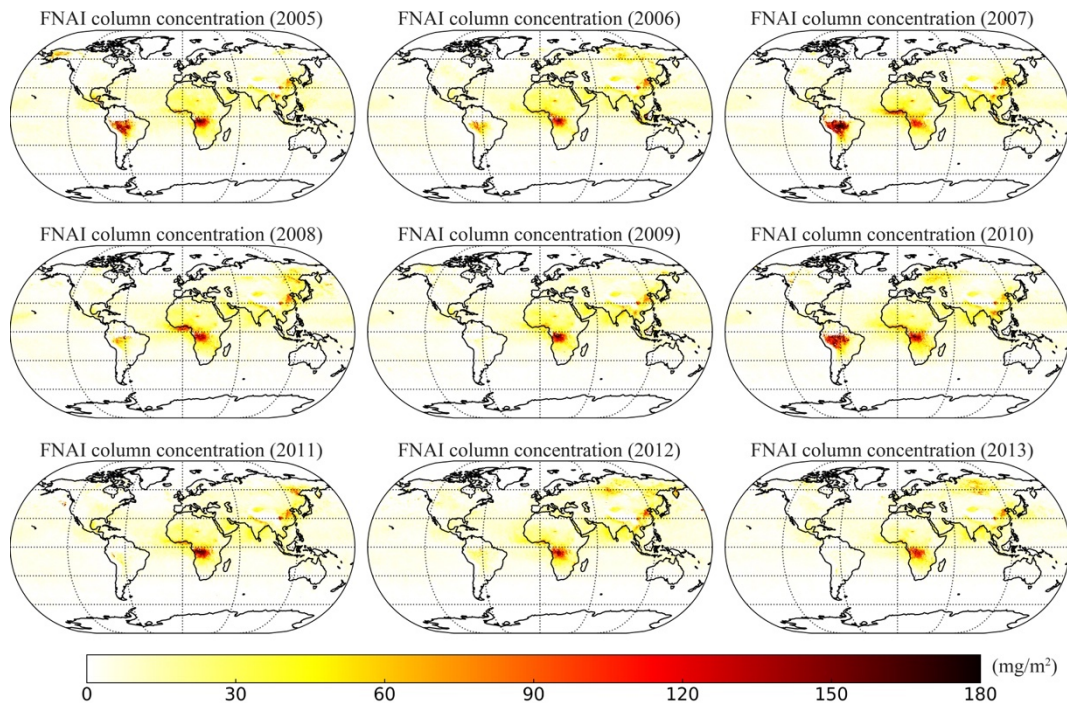
Figure 16: Yearly mean of FNAI ~~columnar~~ column mass concentration (mg/m^2) ~~in a resolution of 0.1° × 0.1°~~ derived by the GRASP/Component approach from POLDER-3 observations for the period from March 2005 to October 2013.

3.2.3 Non-Absorbing Soluble (NAS) and Aerosol Water Content (AWC)

As aforementioned and discussed in Li et al. (2019), the components contained in the host can represent all of ammonium nitrate, sulfate, sea salt and aerosol water content in fine- and coarse-mode aerosol fraction. However, the NAS also can be aged hydroscopic components such as water-soluble organic carbon generated from biomass burning or anthropogenic activities, and water-soluble mineral ions provided by dust particles. The NAS and AWC components thus can be quite complex for interpretation, however, overall the obtained climatology presents a reasonable logic. For example, fine-mode non-absorbing soluble component (FNAS, in Fig. 17) is high in China and India, especially during the DJF and SON season that is in line with strong anthropogenic emissions (e.g., industrial and heating activity)

in megacities where the population is dense. The non-absorbing water-soluble organic carbon, that can be emitted during biomass burning events, can be also detected and interpreted as FNAS, e.g., as it occurs in southern Africa. The GRASP/Component retrievals also indicate many NAS particles present in the Mediterranean region, which is in line with the previously demonstrated aerosol mixture constituted of anthropogenic aerosols, sea salt particles, and mineral dust coated with biogenic sulfate (Ganor et al., 2000; Lelieveld et al., 2002; Levin, 2005; Levin et al., 1996). The spatio-temporal distributions of aerosol water content appear to be similar to the non-absorbing soluble component, which is quite logical because these two components are naturally related and also form the particle host in the employed Maxwell-Garnet effective medium approximation mixing rule in the algorithm. The fine-mode aerosol water content (Fig. 18) is also naturally associated with hygroscopic anthropogenic aerosol particles and dominates in regions such as Asia. The aerosol water presence over ocean during the dust transport and near southern Africa during the biomass burning is also rather logical because of higher atmospheric relative humidity.

~~Moreover, possible the hygroscopicity of aged dust was reported in several studies (Sullivan et al., 2009; Tang et al., 2016) and the signal can also appear in observations (Derimian et al., 2017; Falkovich et al., 2004).~~ Moreover, a significant increase of mineral dust hygroscopicity was attributed in several studies to the aging processes and the dust mixing with soluble hygroscopic material (Sullivan et al., 2009; Tang et al., 2016). Impact of such mixtures on remote sensing observations was also observed (Derimian et al., 2017; Falkovich et al., 2004). Besides some regions with high coarse-mode non-absorbing insoluble (dust) concentration over ocean (near western Africa and Arabian Peninsula), the values of NAS and AWC in coarse mode are rather low everywhere. We note that a relatively low fraction but with very large volume concentration could produce relatively important concentration. In addition, in situations when the real part of aerosol refractive index is very low, the algorithm may try to introduce a water fraction and thus produce an artefact. This is rather the case when a water fraction is retrieved over the Bodélé Depression during the DJF season. Indeed, an important proportion of fossil diatom in the sediments of the Bodélé Depression (Formenti et al., 2008) can produce dust with unusually low real part of refractive index. To reproduce the optical signal of this dust, a small fraction of water can be required (element with the lowest real refractive index). Since the dust concentrations are extremely high in this

690 source, even small fraction presents relatively high water concentrations, which is an artefact. This example illustrates that interpretations of the retrieved component fractions are not always straightforward and depend on limits in the measurement sensitivity. Nevertheless, the measurements reflecting physical properties and a closer analysis can usually explain mismatches with expectations.
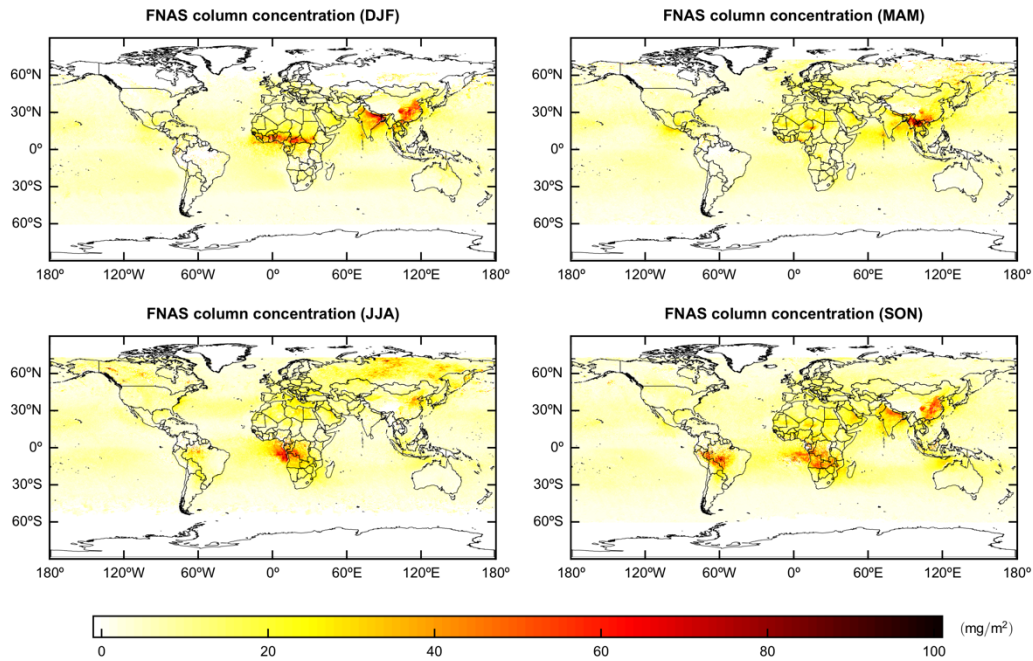
695 **Figure 17:** Spatial distribution of ~~0.1° × 0.1°~~ seasonal FNAS (Fine mode Non-Absorbing Soluble component) ~~columnar~~ column mass concentration (mg/m²) derived by the GRASP/Component approach from POLDER-3 observations. DJF: December-January-February; MAM: March-April-May; JJA: June-July-August; SON: September-October-November.
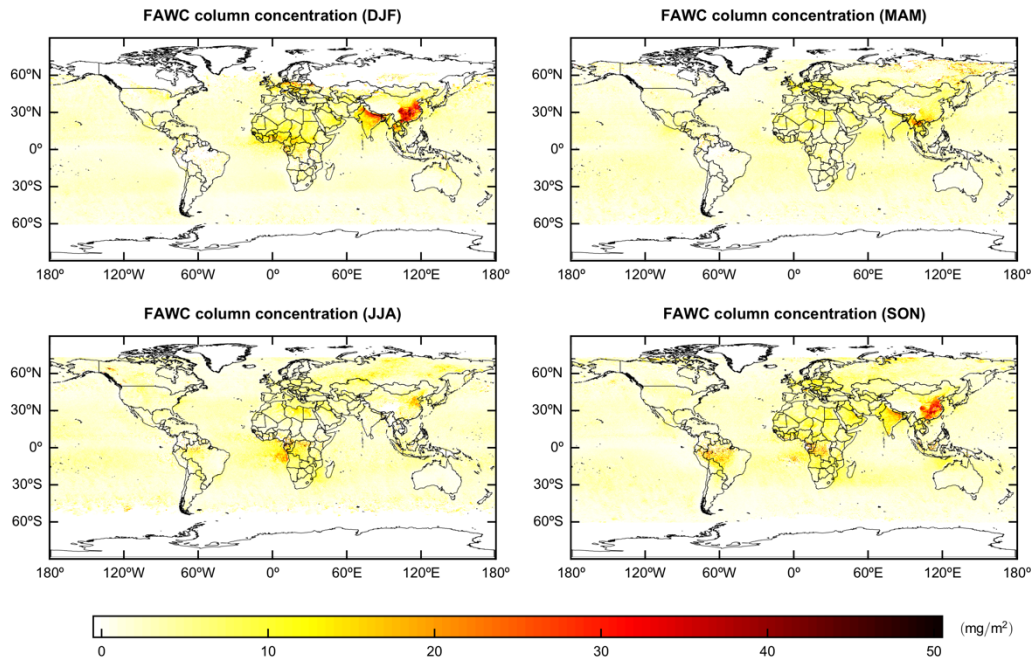
700

Figure 18: Spatial distribution of ~~0.1° × 0.1°~~ seasonal FAWC (Fine mode Aerosol Water Content) ~~columnar~~ column mass concentration (mg/m^2) derived by the GRASP/Component approach from POLDER-3 observations. DJF: December-January-February; MAM: March-April-May; JJA: June-July-August; SON: September-October-November.

4 Comparisons of BC and dust concentration derived by GRASP/Component with MERRA-2

Although applications of GRASP/Component to different instruments (sun photometer, POLDER-3, DPC/GF-5) have presented good consistency with the available AERONET aerosol optical products such as AOD, AAOD, AE and also agree with the physical expectations about aerosol composition in different locations, an addition reference data are still desirable for the validation. Because the in situ measurements data are extremely scarce and difficult for global validation, we employ an inter-comparison of BC and dust ~~columnar~~ column concentration between GRASP/Component climatological dataset and the corresponding MERRA-2 products. Indeed, this is not a pure validation experiment, but can still provide

a better indicator of a global consistency. The CNAI component here we will refer to the dust component in MERRA-2. The GRASP/Component dust and also BC products will be inter-compared. To this end, the GRASP/Component products are re-gridded into the same resolution of 0.5° × 0.625° as of MERRA-2. Fig. 19 presents the differences of monthly BC ~~columnar~~ column concentration between GRASP/Component and MERRA-2 for the period March 2005 – October 2013. One can note that both GRASP/Component BC and MERRA-2 BC represent quite similar spatio-temporal pattern and generally show reasonable consistency between them over ocean, Europe, United States, and mostly over South America and Africa, except however some noticeable differences during strong biomass burning season and strong anthropogenic emissions in China and India. In further discussion, we analyze the possible source of these discrepancies.

First, MERRA-2 includes the estimations of several externally mixed aerosol components (e.g., BC, OC, dust, etc.) as defined in the Goddard Chemistry, Aerosol, Radiation, and Transport model (GOCART) (Chin et al., 2002). The emissions for carbonaceous aerosol species in GOCART include fossil fuel combustion, biomass burning, biofuel consumption, and biogenic sources. Both natural and anthropogenic sources make contributions to BC emissions in MERRA-2. Various inventories during the different time periods were considered to produce biomass burning emissions of carbonaceous aerosols in MERRA-2. Specifically, the Quick Fire Emissions Dataset (QFED) version 2.4-r6 (Darmenov and da Silva, 2015) has been employed for daily biomass burning BC emission since 2010. The monthly biomass burning emissions in Global Fire Emission Dataset (GFED) version 3.1 (Randerson et al., 2006; Van Der Werf et al., 2006) were used for the period 1997 – 2009. Biome-dependent factors are used to make corrections between GFED v3.1 and QFED v2.4-r6 during the period 2003 – 2011 when they were available. On the other hand, it is noted that more and more strict controls on air pollution in China have taken with the rapid economic growth (Zhang et al., 2019). The inventory of Peking university (PKU) indicated anthropogenic aerosol emissions present decrease in the key regions of China since 2006 with a significant trend of -1.4% per year for anthropogenic BC emissions during the period 2006 – 2014 (Wang et al., 2021). However, a continuous increase of anthropogenic aerosol emissions in China from 2006 to 2014 is shown in the Community Emissions Data System (CEDS) inventory, thus the global

climate models cannot capture the observed downward trend well (Wang et al., 2021). The comparisons of biomass burning emission datasets including GFED3.1 (Global Fire Emissions Database version 3.1), GFED4s (GFED version 4 with small fires), FINN1.5 (FIre INventory from NCAR version 1.5), GFAS1.2 (Global Fire Assimilation System version 1.2), FEER1.0 (Fire Energetics and Emissions Research version 1.0), and QFED2.4 (Quick Fire Emissions Dataset version 2.4) for 2008 globally have indicated that a factor of 3.4 can be obtained on an annual average for the differences of BC emissions (Pan et al., 2020). At the same time, the knowledge on the complexity and variability of different fire features are still required to be improved (Hyer et al., 2011). Continuous measurements are required to contribute toward advancing our understanding of the fire-generated BC globally, at least in the major biomass burning regions. The emission factors for different ecosystem types and burning stages are needed to be estimated accurately for the improvement of emission globally (Pan et al., 2020).

Second, a higher value of BC refractive index ($1.95 - 0.79i$) employed in the GRASP/Component for the BC retrievals (Li et al., 2019) than BC refractive index ($1.75 - 0.45i$) used in the GOCART model (Chin et al., 2002), which affects the GRASP BC mass retrievals, also makes contributions to the BC differences. Finally, we also should note that a new light-absorbing carbonaceous component, named BrC, is included in the GRASP/Component products so that the spectral aerosol absorption signature in the fine-mode fraction can be interpreted as BrC contribution in the satellite inversion. Whereas at present MERRA-2 do not provide BrC product. Therefore, for instance, the noticeable BrC concentrations over ocean near the southern Africa for the strong biomass burning season (in Fig. 5) can indeed explain the BC underestimation by GRASP/Component relative to MERRA-2. The comparisons of GOCART BrC estimations (Schill et al., 2020) and GRASP BrC retrievals are expected to be done in a future study.

The monthly dust ~~columnar~~ column concentration differences between GRASP/Component and MERRA-2 for the period March 2005 – October 2013 are presented in Fig. 20. We can see that GRASP/Component dust concentration is less than one of MERRA-2 over the northern Africa, Arabian Peninsula, Middle Asia, and northwest China. We would like to recall that the wind speed-dependent emissions with the potential dust source locations described in Ginoux et al. (2001) are used for dust missions in the MERRA-2/GOCART model and that the depositions (such as dry deposition, wet removal globally) of aerosol are not considered in the current GOCART estimation for MERRA-2 (Randles et al.,

2017). These factors can cause the overestimation of dust in MERRA-2. At the same time, the
770 GRASP/Component dust concentration used for the comparison represent the CNAI (coarse-mode non-
absorbing insoluble component) concentration that excludes the fine-mode dust and absorbing that leads
to a systematic underestimation of the dust component as it is defined in MERRA-2. These differences
can merit a closer future analysis as function of dust source region, composition and transport distance.
We note that GRASP CNAI retrieval shows slightly higher than MERRA-2 dust in the southern Africa,
775 which might be related to the probably existing coarse-mode organic particles during the biomass burning
seasons with strong carbonaceous aerosol emissions.
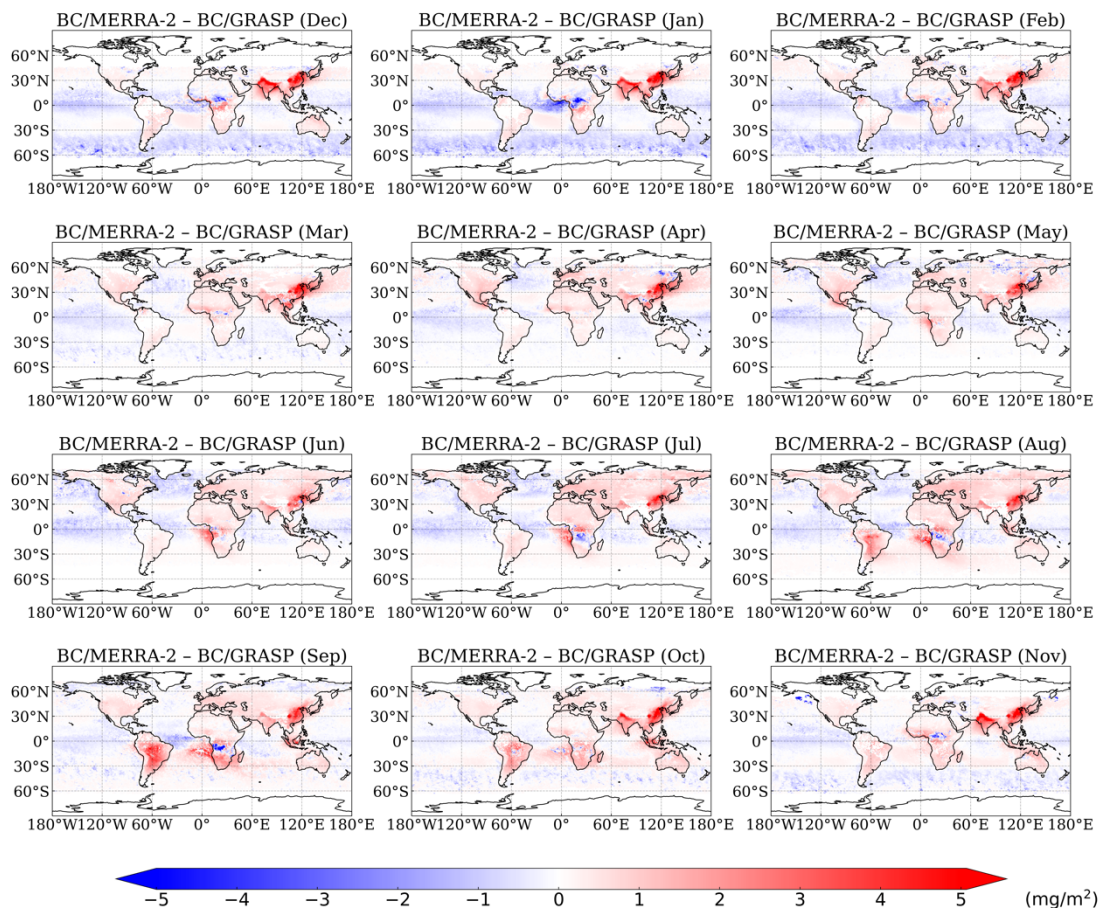
Figure 19: Differences of monthly BC ~~columnar~~ column concentration between GRASP/Component and
780 MERRA-2 in the resolution of 0.5° × 0.625° for the period March 2005 – October 2013.
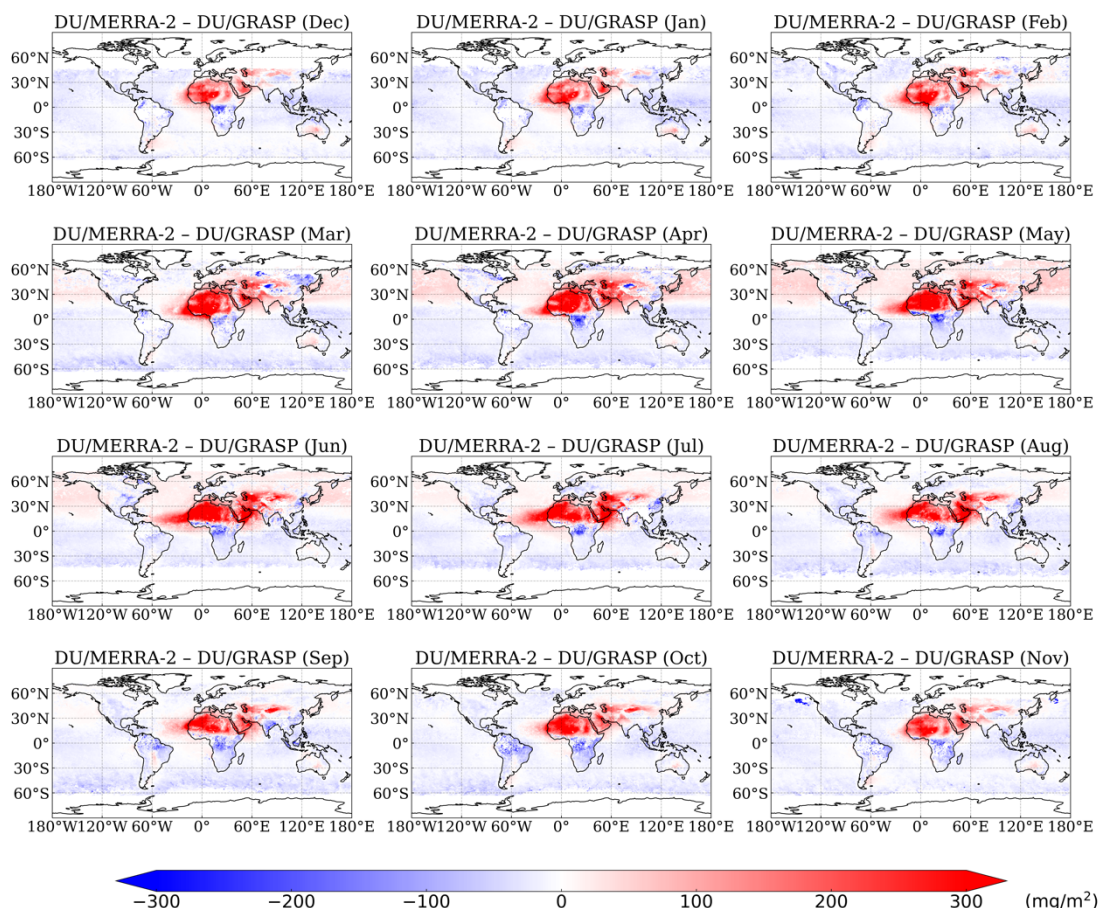
Figure 20: Differences of monthly dust ~~columnar~~ column concentration between GRASP/Component and MERRA-2 in the resolution of 0.5° × 0.625° for the period March 2005 – October 2013.

5 Data availability

The GRASP/Component products derived from POLDER-3 are publicly available on the GRASP algorithm website (https://www.grasp-open.com/products, last access: 15 March 2022). The monthly MERRA-2 BC and dust ~~columnar~~ column concentration products are available at NASA website

6 Conclusions

795 The current paper presents a climatological analysis of the aerosol product recently generated from POLDER-3 by newly developed GRASP/Component approach. This approach employs an essentially different, compared to previous algorithms, methodology and attempts to derive not only optical properties of aerosol and also some information about aerosol composition. The GRASP/Component algorithm provides global satellite observations based concentrations of absorbing components such as

800 BC, BrC, CAI representing iron oxides contained in dust, and of scattering components such as fine mode organic carbon/scattering dust and coarse mode scattering dust, which is a scarce but imperative information required for tuning the chemical transport models. This GRASP generated satellite-derived aerosol component product is expected to be valuable for qualitative and quantitative understanding of aerosol components distribution on global and regional scales. ~~More importantly, the data assimilation of~~

805 ~~the derived fractions of different aerosol components into the chemical transport models can provide an important constraint for improving the aerosol modeling simulations and reduce some regional inconsistency among climate models.~~ More importantly, the data assimilation of this extensive satellite-based aerosol component dataset can importantly contribute to improving global aerosol emissions estimation and further improvement of accuracy of the estimated aerosol radiative forcing in general and

810 per aerosol component in particular. For instance, the AOD and the AAOD products derived from POLDER-3 observations have been already used to constrain GEOS-Chem inverse modeling for the improvement of global black carbon, organic carbon and desert dust aerosol emissions (Chen et al., 2018, 2019). Using the presented in this study additional satellite-based aerosol component products, the further improvement of global aerosol emissions estimation is thus expected. The presented efforts are also in

815 line with the studies suggesting that the employment of satellite-constrained anthropogenic and natural aerosol emissions by the climate models is required to improve the accuracy of aerosol radiative forcing

estimations (e.g., Bellouin et al., 2020; Quaas et al., 2022). That is, the linear trends in column concentration of the main aerosol components, such as BC, BrC, CAI and CNAI as shown in Fig. S1 in the supplement, can provide a better global scale satellite-measured constraints on the properties of anthropogenic (BC and BrC) and natural (CAI and CNAI) aerosols and will contribute to improving the accuracy of anthropogenic aerosol radiative forcing estimations. This paper show and disuses the climatological patterns derived from POLDER-3 using GRASP/Component approach. It is shown that this global satellite derived aerosol chemical composition climatology clearly reveals the distribution of global dust belt, biomass burning events, and anthropogenic activity emissions that is in good agreement with known logical expectations and previous studies. The inter-comparisons of BC and dust ~~columnar~~ column concentrations provided by GRASP/Component and MERRA-2 for the period March 2005 – October 2013 show good agreement in global spatio-temporal patterns, although some explainable differences appear for strong biomass burning events and in regions strongly affected by mineral dust. For example, the BC emissions can affect significantly the MERRA-2 BC concentrations during the strong biomass burning periods.

In addition, all GRASP/Component generated optical properties agree very closely with the best previously obtained POLDER-3 aerosol products not only over AERONET stations and also globally both over land and over ocean. Specifically, the GRASP/Component approach is demonstrated to provide the aerosol optical characteristics of comparable or sometimes even better accuracy (as validated by AERONET data) as all other earlier GRASP/Optimized, High Precision and Models products. For example, the validation study by Zhang et al. (2021b) using global AEROENT data shown that total spectral AOD quite closely agrees with GRASP/Models retrieval that has highest correlation and lowest bias (Chen et al., 2020). At the same time, most of the GRASP/Component detailed characteristics (spectral AODF, AODC, AAOD and SSA) provided by GRASP/Component also agree well with the aerosol optical products of previous GRASP approaches (Optimized, High Precision, and Models) in Chen et al. (2020).

Although a rigorous global validation of aerosol component remains challenging at the current stage, its estimation is the next frontier for the aerosol inversion from satellite observation because is required for continuous evaluation of aerosol life cycle by chemical transport models. Also, it should be pointed out that in situ aerosol component data are scarce unlike satellite AOD products on global scale. The presented here satellite aerosol component product is comparable in coverage with conventional AOD product, whole retrieval require more complex aerosol parameterization and advanced remote sensing observations such as the multi-angular polarimetric observations. At the same time, many space-borne instruments with the multi-angle polarization measurement capabilities are planned to be deployed and available in the next few years (Dubovik et al., 2019), such as 3MI (Multi-View Multi-Channel Multi-Polarization Imaging), DPC-02 (Directional Polarimetric Camera) etc. Finally, the presented work illustrates that with the synergy of different remote sensing instruments and additional algorithm refinements allow the extensive retrievals of aerosol microphysical and optical properties together with aerosol composition information, as derived by GRASP/Component algorithm, can be extensively generated in the near future.

Supplement

Table S1. The definitions and descriptions of aerosol components with their complex refractive indices at 440 nm and 865 nm.

Component	Complex refractive index		Reference
	0.440 μm	0.865 μm	
BC represents wavelength-independent strong absorption	1.95+0.79i	1.95+0.79i	Bond and Bergstrom (2006)
	1.75+0.63i	1.75+0.63i	Bond and Bergstrom (2006)
BrC represents wavelength-dependent absorption	1.54+0.07i	1.54+0.003i	Sun et al. (2007)
	1.54+0.06i	1.54+0.0005i	Kirchstetter et al. (2004)
CAI mainly represents iron oxides contained in the coarse-mode dust particles	2.90+0.345i	2.75+0.003i	Longtin et al. (1988)
	2.88+0.987i	2.72+0.140i	Triaud (2005)
CNAI mainly represents coarse-mode non-absorbing dust particles	1.54+0.0005i	1.52+0.0005i	Ghosh (1999)
	1.53+0.005i	1.53+0.005i	Ghosh (1999); Sokolik and Toon (1999); Journet et al. (2014)
FNAI represents fine-mode non-absorbing insoluble dust and organic carbon	1.54+0.0005i	1.52+0.0005i	Ghosh (1999)
	1.53+0.005i	1.53+0.005i	Ghosh (1999); Sokolik and Toon (1999); Journet et al. (2014)

FNAS represents fine-mode inorganic salts	$1.337+10^{-9}i$	$1.339+10^{-8}i$	Tang et al. (1981); Gosse et al. (1997)
FAWC represents fine-mode aerosol water content	$1.337+10^{-9}i$	$1.329+10^{-6.5}i$	Hale and Querry (1973)

865
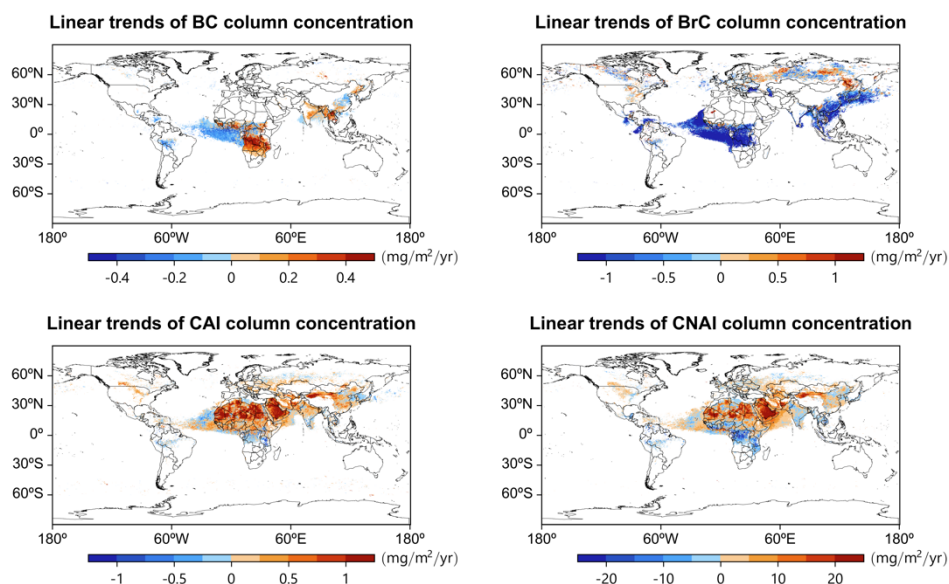
Fig S1. Linear trends in column concentration of BC, BrC, CAI and CNAI components with the criteria of AOD (440 nm) > 0.2 and for BC (> 1 mg/m^2), BrC (> 10 mg/m^2), CAI (> 2 mg/m^2), and CANI (> 50

870   mg/m^2).

Author contributions. The GRASP/Component approach was developed by the GRASP team (OD, LL, YD, GS, DF, PL, TL, AL, CC, FD, YK, BT). LL, YD, HC and OD carried out this study and analysis.

875   CC, XZ, CM, KG, YZ and YL contributed to the post-processed retrievals and the figures. The component

products were widely discussed with some modeler, who are co-authors of this paper. LL, HC and OD wrote the manuscript with contributions from all authors.

Competing interests. The authors declare that they have no conflict of interest.

Acknowledgements. The authors would like to acknowledge the use of POLDER-3 Level-1 data originally provided by CNES. The authors are also grateful to the MERRA-2 product team.

Financial support. This research has been supported by the National Science Fund for Distinguished Young Scholars (41825011), the National Natural Science Foundation of China (41905117 & 42030608), the National Key Research and Development Program (2019YFC0214603). The component algorithm was developed as part of the Labex CaPPA project, which is funded by the Agence Nationale de la Recherche (grant no. ANR-II-LABX-0005-01).

References

Adachi, K. and Buseck, P. R.: Changes of ns-soot mixing states and shapes in an urban area during CalNex, J. Geophys. Res. Atmos., 118(9), 3723–3730, doi:10.1002/jgrd.50321, 2013.

Alizadeh-Choobari, O., Zawar-Reza, P. and Sturman, A.: The „wind of 120days" and dust storm activity over the Sistan Basin, Atmos. Res., 143, 328–341, doi:10.1016/j.atmosres.2014.02.001, 2014.

Arola, A., Schuster, G., Myhre, G., Kazadzis, S., Dey, S. and Tripathi, S. N.: Inferring absorbing organic carbon content from AERONET data, Atmos. Chem. Phys., 11(1), 215–225, doi:10.5194/acp-11-215-2011, 2011.

Bahadur, R., Praveen, P. S., Xu, Y. and Ramanathan, V.: Solar absorption by elemental and brown carbon determined from spectral observations, Proc. Natl. Acad. Sci., 109(43), 17366–17371, doi:10.1073/pnas.1205910109, 2012.

Bellouin, N., Boucher, O., Haywood, J. and Reddy, M. S.: Global estimate of aerosol direct radiative forcing from satellite measurements, Nature, 438(7071), 1138–1141, doi:10.1038/nature04348, 2005.

Bellouin, N., Davies, W., Shine, K. P., Quaas, J., Mülmenstädt, J., Forster, P. M., Smith, C., Lee, L.,
900 Regayre, L., Brasseur, G., Sudarchikova, N., Bouarar, I., Boucher, O., and Myhre, G.: Radiative forcing
of climate change from the Copernicus reanalysis of atmospheric composition, Earth Syst. Sci. Data, 12,
1649–1677, doi: 10.5194/essd-12-1649-2020, 2020.

Bellouin, N., Quaas, J., Gryspeerdt, E., Kinne, S., Stier, P., Watson-Parris, D., Boucher, O., Carslaw, K.
S., Christensen, M., Daniau, A. L., Dufresne, J. L., Feingold, G., Fiedler, S., Forster, P., Gettelman, A.,
905 Haywood, J. M., Lohmann, U., Malavelle, F., Mauritsen, T., McCoy, D. T., Myhre, G., Mülmenstädt, J.,
Neubauer, D., Possner, A., Rugenstein, M., Sato, Y., Schulz, M., Schwartz, S. E., Sourdeval, O.,
Storelvmo, T., Toll, V., Winker, D. and Stevens, B.: Bounding Global Aerosol Radiative Forcing of
Climate Change, Rev. Geophys., 58(1), 1–45, doi:10.1029/2019RG000660, 2020.

Benavent-Oltra, J. A., Román, R., Casquero-Vera, J. A., Pérez-Ramírez, D., Lyamani, H., Ortiz-
910 Amezcua, P., Bedoya-Velásquez, A. E., de Arruda Moreira, G., Barreto, Á., Lopatin, A., Fuertes, D.,
Herrera, M., Torres, B., Dubovik, O., Guerrero-Rascado, J. L., Goloub, P., Olmo-Reyes, F. J. and Alados-
Arboledas, L.: Different strategies to retrieve aerosol properties at night-time with the GRASP algorithm,
Atmos. Chem. Phys., 19(22), 14149–14171, doi:10.5194/acp-19-14149-2019, 2019.

Bohren, C. F. and Huffman, D. R.: Scattering Coefficients, Absorption and scattering of light by small
915 particles., 1983.

Bond, T. C. and Bergstrom, R. W.: Light Absorption by Carbonaceous Particles: An Investigative
Review, Aerosol Sci. Technol., 40(1), 27–67, doi:10.1080/02786820500421521, 2006.

Bond, T. C., Doherty, S. J., Fahey, D. W., Forster, P. M., Berntsen, T., Deangelo, B. J., Flanner, M. G.,
Ghan, S., Kärcher, B., Koch, D., Kinne, S., Kondo, Y., Quinn, P. K., Sarofim, M. C., Schultz, M. G.,
920 Schulz, M., Venkataraman, C., Zhang, H., Zhang, S., Bellouin, N., Guttikunda, S. K., Hopke, P. K.,
Jacobson, M. Z., Kaiser, J. W., Klimont, Z., Lohmann, U., Schwarz, J. P., Shindell, D., Storelvmo, T.,
Warren, S. G. and Zender, C. S.: Bounding the role of black carbon in the climate system: A scientific
assessment, J. Geophys. Res. Atmos., 118(11), 5380–5552, doi:10.1002/jgrd.50171, 2013.

Bréon, F. M., Vermeulen, A. and Descloitres, J.: An evaluation of satellite aerosol products against
925 sunphotometer measurements, Remote Sens. Environ., 115(12), 3102–3111,
doi:10.1016/j.rse.2011.06.017, 2011.

Buchard, V., da Silva, A. M., Randles, C. A., Colarco, P., Ferrare, R., Hair, J., Hostetler, C., Tackett, J. and Winker, D.: Evaluation of the surface PM2.5 in Version 1 of the NASA MERRA Aerosol Reanalysis over the United States, Atmos. Environ., 125, 100–111, doi:10.1016/j.atmosenv.2015.11.004, 2016.

930 Buchard, V., Randles, C. A., da Silva, A. M., Darmenov, A., Colarco, P. R., Govindaraju, R., Ferrare, R., Hair, J., Beyersdorf, A. J., Ziemba, L. D. and Yu, H.: The MERRA-2 aerosol reanalysis, 1980 onward. Part II: Evaluation and case studies, J. Clim., 30(17), 6851–6872, doi:10.1175/JCLI-D-16-0613.1, 2017.

Buriez, J. C., Vanbauce, C., Parol, F., Goloub, P., Herman, M., Bonnel, B., Fouquart, Y., Couvert, P. and Seze, G.: Cloud detection and derivation of cloud properties from POLDER, Int. J. Remote Sens., 18(13),

935 2785–2813, doi:10.1080/014311697217332, 1997.

Burton, S. P., Ferrare, R. A., Hostetler, C. A., Hair, J. W., Rogers, R. R., Obland, M. D., Butler, C. F., Cook, A. L., Harper, D. B. and Froyd, K. D.: Aerosol classification using airborne High Spectral Resolution Lidar measurements-methodology and examples, Atmos. Meas. Tech., 5(1), 73–98, doi:10.5194/amt-5-73-2012, 2012.

940 Burton, S. P., Vaughan, M. A., Ferrare, R. A. and Hostetler, C. A.: Separating mixtures of aerosol types in airborne High Spectral Resolution Lidar data, Atmos. Meas. Tech., 7(2), 419–436, doi:10.5194/amt-7-419-2014, 2014.

Cazorla, A., Bahadur, R., Suski, K. J., Cahill, J. F., Chand, D., Schmid, B., Ramanathan, V. and Prather, K. A.: Relating aerosol absorption due to soot, organic carbon, and dust to emission sources determined

945 from in-situ chemical measurements, Atmos. Chem. Phys., 13(18), 9337–9350, doi:10.5194/acp-13-9337-2013, 2013.

Chakrabarty, R. K., Moosmüller, H., Chen, L. W. A., Lewis, K., Arnott, W. P., Mazzoleni, C., Dubey, M. K., Wold, C. E., Hao, W. M. and Kreidenweis, S. M.: Brown carbon in tar balls from smoldering biomass combustion, Atmos. Chem. Phys., 10(13), 6363–6370, doi:10.5194/acp-10-6363-2010, 2010.

950 Chen, C., Dubovik, O., Henze, D. K., Lapyonak, T., Chin, M., Ducos, F., Litvinov, P., Huang, X. and Li, L.: Retrieval of desert dust and carbonaceous aerosol emissions over Africa from POLDER/PARASOL products generated by the GRASP algorithm, Atmos. Chem. Phys., 18(16), 12551–12580, doi:10.5194/acp-18-12551-2018, 2018.

Chen, C., Dubovik, O., Henze, D. K., Chin, M., Lapyonok, T., Schuster, G. L., Ducos, F., Fuertes, D.,

Litvinov, P., Li, L., Lopatin, A., Hu, Q. and Torres, B.: Constraining global aerosol emissions using POLDER/PARASOL satellite remote sensing observations, Atmos. Chem. Phys., 19(23), 14585–14606, doi:10.5194/acp-19-14585-2019, 2019.

Chen, C., Dubovik, O., Fuertes, D., Litvinov, P., Lapyonok, T., Lopatin, A., Ducos, F., Derimian, Y., Herman, M., Tanré, D., Remer, L. A., Lyapustin, A., Sayer, A. M., Levy, R. C., Christina Hsu, N., Descloitres, J., Li, L., Torres, B., Karol, Y., Herrera, M., Herreras, M., Aspetsberger, M., Wanzenboeck, M., Bindreiter, L., Marth, D., Hangler, A. and Federspiel, C.: Validation of GRASP algorithm product from POLDER/PARASOL data and assessment of multi-angular polarimetry potential for aerosol monitoring, Earth Syst. Sci. Data, 12(4), 3573–3620, doi:10.5194/essd-12-3573-2020, 2020.

Chen, W. T., Kahn, R. A., Nelson, D., Yau, K. and Seinfeld, J. H.: Sensitivity of multiangle imaging to the optical and microphysical properties of biomass burning aerosols, J. Geophys. Res. Atmos., 113(10), 1–22, doi:10.1029/2007JD009414, 2008.

Chin, M., Ginoux, P., Kinne, S., Torres, O., Holben, B. N., Duncan, B. N., Martin, R. V., Logan, J. A., Higurashi, A. and Nakajima, T.: Tropospheric Aerosol Optical Thickness from the GOCART Model and Comparisons with Satellite and Sun Photometer Measurements, J. Atmos. Sci., 59(3), 461–483, 2002.

China, S., Mazzoleni, C., Gorkowski, K., Aiken, A. C. and Dubey, M. K.: Morphology and mixing state of individual freshly emitted wildfire carbonaceous particles, Nat. Commun., 4(1), 2122, doi:10.1038/ncomms3122, 2013.

Choobari, O. A., Zawar-Reza, P. and Sturman, A.: The global distribution of mineral dust and its impacts on the climate system: A review, Atmos. Res., 138, 152–165, doi:10.1016/j.atmosres.2013.11.007, 2014.

Chung, C. E., Ramanathan, V. and Decremer, D.: Observationally constrained estimates of carbonaceous aerosol radiative forcing, Proc. Natl. Acad. Sci., 109(29), 11624–11629, doi:10.1073/pnas.1203707109, 2012.

Clarisse, L., Clerbaux, C., Franco, B., Hadji-Lazaro, J., Whitburn, S., Kopp, A. K., Hurtmans, D. and Coheur, P. F.: A Decadal Data Set of Global Atmospheric Dust Retrieved From IASI Satellite Measurements, J. Geophys. Res. Atmos., 124(3), 1618–1647, doi:10.1029/2018JD029701, 2019.

Costabile, F., Barnaba, F., Angelini, F. and Gobbi, G. P.: Identification of key aerosol populations through their size and composition resolved spectral scattering and absorption, Atmos. Chem. Phys., 13(5), 2455–

2470, doi:10.5194/acp-13-2455-2013, 2013.

Cox, C. and Munk, W.: Measurement of the Roughness of the Sea Surface from Photographs of the Sun's Glitter, J. Opt. Soc. Am., 44(11), 838, doi:10.1364/JOSA.44.000838, 1954.

Darmenov, A. and da Silva, A. M.: The Quick Fire Emissions Dataset (QFED) - Documentation of versions 2.1, 2.2 and 2.4., NASA Tech. Rep. Ser. Glob. Model. Data Assim., 32(September), 2015.

Decesari, S., Facchini, M. C., Matta, E., Mircea, M., Fuzzi, S., Chughtai, A. R. and Smith, D. M.: Water soluble organic compounds formed by oxidation of soot, Atmos. Environ., 36(11), 1827–1832, doi:10.1016/S1352-2310(02)00141-3, 2002.

Derimian, Y., Karnieli, A., Kaufman, Y. J., Andreae, M. O., Andreae, T. W., Dubovik, O., Maenhaut, W. and Koren, I.: The role of iron and black carbon in aerosol light absorption, Atmos. Chem. Phys., 8, 3632–3637 [interaktyvus] Available from: http://www.atmos-chem-phys.net/8/3623/2008/, 2008.

Derimian, Y., Marie Cho, I., Rudich, Y., Deboudt, K., Dubovik, O., Laskin, A., Legrand, M., Damiri, B., Koren, I., Unga, F., Moreau, M., Andreae, M. and Karnieli, A.: Effect of sea breeze circulation on aerosol mixing state and radiative properties in a desert setting, Atmos. Chem. Phys., 17(18), 11331–11353, doi:10.5194/acp-17-11331-2017, 2017.

Deschamps, P. Y., Buriez, J. C., Bréon, F. M., Leroy, M., Podaire, A., Bricaud, A. and Sèze, G.: The POLDER Mission: Instrument Characteristics and Scientific Objectives, IEEE Trans. Geosci. Remote Sens., 32(3), 598–615, doi:10.1109/36.297978, 1994.

Deuzé, J. L., Bréon, F. M., Devaux, C., Goloub, P., Herman, M., Lafrance, B., Maignan, F., Marchand, A., Nadal, F., Perry, G. and Tanré, D.: Remote sensing of aerosols over land surfaces from POLDER-ADEOS-1 polarized measurements, J. Geophys. Res. Atmos., 106(D5), 4913–4926, doi:10.1029/2000JD900364, 2001.

Dey, S., Tripathi, S. N., Singh, R. P. and Holben, B. N.: Retrieval of black carbon and specific absorption over Kanpur city, northern India during 2001-2003 using AERONET data, Atmos. Environ., 40(3), 445–456, doi:10.1016/j.atmosenv.2005.09.053, 2006.

Dubovik, O.: Optimization of Numerical Inversion in Photopolarimetric Remote Sensing, Photopolarimetry in Remote Sensing, t. 161, p. 65–106, Kluwer Academic Publishers, Dordrecht., 2004.

Dubovik, O. and King, M. D.: A flexible inversion algorithm for retrieval of aerosol optical properties

from Sun and sky radiance measurements, J. Geophys. Res. Atmos., 105(D16), 20673–20696, doi:10.1029/2000JD900282, 2000.

Dubovik, O., Smirnov, A., Holben, B. N., King, M. D., Kaufman, Y. J., Eck, T. F. and Slutsker, I.: Accuracy assessments of aerosol optical properties retrieved from Aerosol Robotic Network (AERONET) Sun and sky radiance measurements, J. Geophys. Res. Atmos., 105(D8), 9791–9806, doi:10.1029/2000JD900040, 2000.

Dubovik, O., Holben, B. N., Lapyonok, T., Sinyuk, A., Mishchenko, M. I., Yang, P. and Slutsker, I.: Non-spherical aerosol retrieval method employing light scattering by spheroids, Geophys. Res. Lett., 29(10), 54-1-54–4, doi:10.1029/2001GL014506, 2002a.

Dubovik, O., Holben, B. N., Eck, T. F., Smirnov, A., Kaufman, Y. J., King, M. D., Tanré, D. and Slutsker, I.: Variability of Absorption and Optical Properties of Key Aerosol Types Observed in Worldwide Locations, J. Atmos. Sci., 59(3), 590–608, 2002b.

Dubovik, O., Sinyuk, A., Lapyonok, T., Holben, B. N., Mishchenko, M., Yang, P., Eck, T. F., Volten, H., Muñoz, O., Veihelmann, B., van der Zande, W. J., Leon, J. F., Sorokin, M. and Slutsker, I.: Application of spheroid models to account for aerosol particle nonsphericity in remote sensing of desert dust, J. Geophys. Res. Atmos., 111(11), 1–34, doi:10.1029/2005JD006619, 2006.

Dubovik, O., Lapyonok, T., Kaufman, Y. J., Chin, M., Ginoux, P., Kahn, R. A. and Sinyuk, A.: Retrieving global aerosol sources from satellites using inverse modeling, Atmos. Chem. Phys., 8, 209–250, doi:10.5194/acp-8-209-2008, 2008.

Dubovik, O., Herman, M., Holdak, A., Lapyonok, T., Tanré, D., Deuzé, J. L., Ducos, F., Sinyuk, A. and Lopatin, A.: Statistically optimized inversion algorithm for enhanced retrieval of aerosol properties from spectral multi-angle polarimetric satellite observations, Atmos. Meas. Tech., 4(5), 975–1018, doi:10.5194/amt-4-975-2011, 2011.

Dubovik, O., Lapyonok, T., Litvinov, P., Herman, M., Fuertes, D., Ducos, F., Torres, B., Derimian, Y., Huang, X., Lopatin, A., Chaikovsky, A., Aspetsberger, M. and Federspiel, C.: GRASP: a versatile algorithm for characterizing the atmosphere, SPIE Newsroom, 2–5, doi:10.1117/2.1201408.005558, 2014.

Dubovik, O., Li, Z., Mishchenko, M. I., Tanré, D., Karol, Y., Bojkov, B., Cairns, B., Diner, D. J.,

Espinosa, W. R., Goloub, P., Gu, X., Hasekamp, O., Hong, J., Hou, W., Knobelspiesse, K. D., Landgraf, J., Li, L., Litvinov, P., Liu, Y., Lopatin, A., Marbach, T., Maring, H., Martins, V., Meijer, Y., Milinevsky, G., Mukai, S., Parol, F., Qiao, Y., Remer, L., Rietjens, J., Sano, I., Stammes, P., Stamnes, S., Sun, X., Tabary, P., Travis, L. D., Waquet, F., Xu, F., Yan, C. and Yin, D.: Polarimetric remote sensing of atmospheric aerosols: Instruments, methodologies, results, and perspectives, J. Quant. Spectrosc. Radiat. Transf., 224, 474–511, doi:10.1016/j.jqsrt.2018.11.024, 2019.

Dubovik, O., Fuertes, D., Litvinov, P., Lopatin, A., Lapyonok, T., Doubovik, I., Xu, F., Ducos, F., Chen, C., Torres, B., Derimian, Y., Li, L., Herreras-Giralda, M., Herrera, M., Karol, Y., Matar, C., Schuster, G. L., Espinosa, R., Puthukkudy, A., Li, Z., Fischer, J., Preusker, R., Cuesta, J., Kreuter, A., Cede, A., Aspetsberger, M., Marth, D., Bindreiter, L., Hangler, A., Lanzinger, V., Holter, C. and Federspiel, C.: A Comprehensive Description of Multi-Term LSM for Applying Multiple a Priori Constraints in Problems of Atmospheric Remote Sensing: GRASP Algorithm, Concept, and Applications, Front. Remote Sens., 2, 1–52, doi:10.3389/frsen.2021.706851, 2021a.

~~Dubovik, O., Fuertes, D., Litvinov, P., Lopatin, A., Lapyonok, T., Doubovik, I., Xu, F., Ducos, F., Chen, C., Torres, B., Derimian, Y., Li, L., Herreras-Giralda, M., Herrera, M., Karol, Y., Matar, C., Schuster, G. L., Espinosa, R., Puthukkudy, A., Li, Z., Fischer, J., Preusker, R., Cuesta, J., Kreuter, A., Cede, A., Aspetsberger, M., Marth, D., Bindreiter, L., Hangler, A., Lanzinger, V., Holter, C. and Federspiel, C.: A Comprehensive Description of Multi-Term LSM for Applying Multiple a Priori Constraints in Problems of Atmospheric Remote Sensing: GRASP Algorithm, Concept, and Applications, Front. Remote Sens., 2, doi:10.3389/frsen.2021.706851, 2021b.~~

Dubovik, O., Schuster, G. L., Xu, F., Hu, Y., Bösch, H., Landgraf, J. and Li, Z.: Grand Challenges in Satellite Remote Sensing, Front. Remote Sens., 2, 1–10 doi:10.3389/frsen.2021.619818, 2021b. ~~c.~~

Duncan, B. N., Martin, R. V., Staudt, A. C., Yevich, R. and Logan, J. A.: Interannual and seasonal variability of biomass burning emissions constrained by satellite observations, J. Geophys. Res., 108(D2), 4100, doi:10.1029/2002JD002378, 2003.

Elguindi, N., Solmon, F. and Turuncoglu, U.: Quantifying some of the impacts of dust and other aerosol on the Caspian Sea region using a regional climate model, Clim. Dyn., 46(1–2), 41–55, doi:10.1007/s00382-015-2566-5, 2016.

Espinosa, W. R., Remer, L. A., Dubovik, O., Ziemba, L., Beyersdorf, A., Orozco, D., Schuster, G., Lapyonok, T., Fuertes, D. and Martins, J. V.: Retrievals of aerosol optical and microphysical properties from Imaging Polar Nephelometer scattering measurements, Atmos. Meas. Tech., 10, 811–824, doi:10.5194/amt-10-811-2017, 2017.

Falkovich, A. H., Schkolnik, G., Ganor, E. and Rudich, Y.: Adsorption of organic compounds pertinent to urban environments onto mineral dust particles, J. Geophys. Res. Atmos., 109(2), doi:10.1029/2003jd003919, 2004.

Flower, V. J. B. and Kahn, R. A.: Distinguishing remobilized ash from erupted volcanic plumes using space-borne multi-angle imaging, Geophysical Research Letters, 44, 10772-10779, doi: 10.1002/2017GL074740, 2017.

Flower, V. J. B. and Kahn, R. A.: Interpreting the volcanological processes of Kamchatka, based on multi-sensor satellite observations, Remote Sensing of Environment, 237, 111585, doi: 10.1016/j.rse.2019.111585, 2020.

Flower, V. J. B. and Kahn, R. A.: Karymsky volcano eruptive plume properties based on MISR multi-angle imagery and the volcanological implications, Atmos. Chem. Phys., 18, 3903-3918, doi: 10.5194/acp-18-3903-2018, 2018.

Flower, V. J. B. and Kahn, R. A.: Twenty years of NASA-EOS multi-sensor satellite oservations at Kilauea volcano (2000 – 2019), Journal of Volcanology and Geothermal Research, 415, 107247, doi: 10.1016/j.jvolgeores.2021.107247, 2021.

Formenti, P., Rajot, J. L., Desboeufs, K., Caquineau, S., Chevaillier, S., Nava, S., Gaudichet, A., Journet, E., Triquet, S., Alfaro, S., Chiari, M., Haywood, J., Coe, H. and Highwood, E.: Regional variability of the composition of mineral dust from western Africa: Results from the AMMA SOP0/DABEX and DODO field campaigns, J. Geophys. Res. Atmos., 113(23), 1–12, doi:10.1029/2008JD009903, 2008.

Formenti, P., Schütz, L., Balkanski, Y., Desboeufs, K., Ebert, M., Kandler, K., Petzold, A., Scheuvens, D., Weinbruch, S. and Zhang, D.: Recent progress in understanding physical and chemical properties of African and Asian mineral dust, Atmos. Chem. Phys., 11(16), 8231–8256, doi:10.5194/acp-11-8231-2011, 2011.

Forster, P., Storelvmo, T., Armour, K. and Collinss, W.: The Earth's energy budget, climate feedbacks,

1095 and climate sensitivity., 2021.

Frouin, R. J., Franz, B. A., Ibrahim, A., Knobelspiesse, K., Ahmad, Z., Cairns, B., Chowdhary, J., Dierssen, H. M., Tan, J., Dubovik, O., Huang, X., Davis, A. B., Kalashnikova, O., Thompson, D. R., Remer, L. A., Boss, E., Coddington, O., Deschamps, P. Y., Gao, B. C., Gross, L., Hasekamp, O., Omar, A., Pelletier, B., Ramon, D., Steinmetz, F. and Zhai, P. W.: Atmospheric Correction of Satellite Ocean-

1100 Color Imagery During the PACE Era, Front. Earth Sci., 7(July), 1–43, doi:10.3389/feart.2019.00145, 2019.

Fu, G. and Hasekamp, O.: Retrieval of aerosol microphysical and optical properties over land using a multimode approach, Atmos. Meas. Tech., 11(12), 6627–6650, doi:10.5194/amt-11-6627-2018, 2018.

Ganguly, D., Ginoux, P., Ramaswamy, V., Dubovik, O., Welton, J., Reid, E. A. and Holben, B. N.:

1105 Inferring the composition and concentration of aerosols by combining AERONET and MPLNET data: Comparison with other measurements and utilization to evaluate GCM output, J. Geophys. Res. Atmos., 114(16), 1–20, doi:10.1029/2009JD011895, 2009a.

Ganguly, D., Ginoux, P., Ramaswamy, V., Winker, D. M., Holben, B. N. and Tripathi, S. N.: Retrieving the composition and concentration of aerosols over the Indo-Gangetic basin using CALIOP and

1110 AERONET data, Geophys. Res. Lett., 36(13), 1–5, doi:10.1029/2009GL038315, 2009b.

Ganor, E., Foner, H. A., Bingemer, H. G., Udisti, R. and Setter, I.: Biogenic sulphate generation in the Mediterranean Sea and its contribution to the sulphate anomaly in the aerosol over Israel and the Eastern Mediterranean, Atmos. Environ., 34(20), 3453–3462, doi:10.1016/S1352-2310(00)00077-7, 2000.

Gelaro, R., McCarty, W., Suárez, M. J., Todling, R., Molod, A., Takacs, L., Randles, C. A., Darmenov,

1115 A., Bosilovich, M. G., Reichle, R., Wargan, K., Coy, L., Cullather, R., Draper, C., Akella, S., Buchard, V., Conaty, A., da Silva, A. M., Gu, W., Kim, G. K., Koster, R., Lucchesi, R., Merkova, D., Nielsen, J. E., Partyka, G., Pawson, S., Putman, W., Rienecker, M., Schubert, S. D., Sienkiewicz, M. and Zhao, B.: The modern-era retrospective analysis for research and applications, version 2 (MERRA-2), J. Clim., 30(14), 5419–5454, doi:10.1175/JCLI-D-16-0758.1, 2017.

1120 Ghosh, G.: Dispersion-equation coefficients for the refractive index and birefringence of calcite and quartz crystals, Opt. Commun., 163, 95–102, doi: 10.1016/S0030-4018(99)00091-7, 1999.

Giles, D. M., Holben, B. N., Eck, T. F., Sinyuk, A., Smirnov, A., Slutsker, I., Dickerson, R. R., Thompson,

A. M. and Schafer, J. S.: An analysis of AERONET aerosol absorption properties and classifications representative of aerosol source regions, J. Geophys. Res. Atmos., 117(17), 1–16, doi:10.1029/2012JD018127, 2012.

Ginoux, P., Chin, M., Tegen, I., Prospero, J. M., Holben, B., Dubovik, O. and Lin, S.-J.: Sources and distributions of dust aerosols simulated with the GOCART model, J. Geophys. Res. Atmos., 106(D17), 20255–20273, doi:10.1029/2000JD000053, 2001.

Ginoux, P., Prospero, J. M., Gill, T. E., Hsu, N. C. and Zhao, M.: Global-scale attribution of anthropogenic and natural dust sources and their emission rates based on MODIS Deep Blue aerosol products, Rev. Geophys., 50(RG3005), 1–36, doi:10.1029/2012RG000388, 2012.

Goloub, P., Chepfer, H., Herman, M., Brogniez, G. and Parol, F.: Use of polarization for cloud study, Polariz. Meas. Anal. Remote Sens., 3121, 330, doi:10.1117/12.283865, 1997.

Goloub, P., Tanré, D., Deuzé, J. L., Herman, M., Marchand, A. and Bréon, F. M.: Validation of the first algorithm applied for deriving the aerosol properties over the ocean using the polder/adeos measurements, IEEE Trans. Geosci. Remote Sens., 37(3 II), 1575–1585, doi:10.1109/36.763268, 1999.

Gosse, S. F., Wang, M., Labrie, D., and Chylek, P.: Imaginary part of the refractive index of sulfates and nitrates in the 0.7-2.6 micron spectral region, Appl. Optics, 36, 3622–3634, 1997.

Goudie, A. S.: Desert dust and human health disorders, Environ. Int., 63, 101–113, doi:10.1016/j.envint.2013.10.011, 2014.

Griffin, D. W., Kellogg, C. A., Garrison, V. H. and Shinn, E. A.: The global transport of dust, Am. Sci., 90(3), 228–235, doi:10.1511/2002.3.228, 2002.

Gui, K., Che, H., Li, L., Zheng, Y., Zhang, L., Zhao, H., Zhong, J., Yao, W., Liang, Y., Wang, Y. and Zhang, X.: The Significant Contribution of Small-Sized and Spherical Aerosol Particles to the Decreasing Trend in Total Aerosol Optical Depth over Land from 2003 to 2018, Engineering, doi:10.1016/j.eng.2021.05.017, 2021a.

Gui, K., Che, H., Zheng, Y., Zhao, H., Yao, W., Li, L., Zhang, L., Wang, H., Wang, Y. and Zhang, X.: Three-dimensional climatology, trends, and meteorological drivers of global and regional tropospheric type-dependent aerosols: insights from 13 years (2007–2019) of CALIOP observations, Atmos. Chem. Phys., 21(19), 15309–15336, doi:10.5194/acp-21-15309-2021, 2021b.

Gui, K., Yao, W., Che, H., An, L., Zheng, Y., Li, L., Zhao, H., Zhang, L., Zhong, J., Wang, Y. and Zhang, X.: Two mega sand and dust storm events over northern China in March 2021: transport processes, historical ranking and meteorological drivers, , (December), 2021c.

Guieu, C., Loÿe-Pilot, M. D., Ridame, C. and Thomas, C.: Chemical characterization of the Saharan dust end-member: Some biogeochemical implications for the western Mediterranean Sea, J. Geophys. Res. Atmos., 107(15), ACH 5-1-ACH 5-11, doi:10.1029/2001JD000582, 2002.

Guo, Y., Tian, B., Kahn, R. A., Kalashnikova, O., Wong, S. and Waliser, D. E.: Tropical Atlantic dust and smoke aerosol variations related to the Madden-Julian Oscillation in MODIS and MISR observations, J. Geophys. Res. Atmos., 118(10), 4947–4963, doi:10.1002/jgrd.50409, 2013.

Hale, G. M. and Querry, M. R.: Optical Constants of Water in the 200-nm to 200-microm Wavelength Region, Appl. Optics, 12, 555–563, doi: 10.1364/AO.12.000555, 1973.

Hasekamp, O. P. and Landgraf, J.: Retrieval of aerosol properties over land surfaces: Capabilities of multiple-viewing-angle intensity and polarization measurements, Appl. Opt., 46(16), 3332–3343, doi:10.1364/AO.46.003332, 2007.

Hasekamp, O. P., Litvinov, P. and Butz, A.: Aerosol properties over the ocean from PARASOL multiangle photopolarimetric measurements, J. Geophys. Res. Atmos., 116(14), 1–13, doi:10.1029/2010JD015469, 2011.

Herman, M., Deuzé, J. L., Marchand, A., Roger, B. and Lallart, P.: Aerosol remote sensing from POLDER/ADEOS over the ocean: Improved retrieval using a nonspherical particle model, J. Geophys. Res. D Atmos., 110(10), 1–11, doi:10.1029/2004JD004798, 2005.

Hsu, N. C., Tsay, S. C., King, M. D. and Herman, J. R.: Deep Blue retrievals of Asian aerosol properties during ACE-Asia, IEEE Trans. Geosci. Remote Sens., 44(11), 3180–3195, doi:10.1109/TGRS.2006.879540, 2006.

Hsu, N. C., Jeong, M. J., Bettenhausen, C., Sayer, A. M., Hansell, R., Seftor, C. S., Huang, J. and Tsay, S. C.: Enhanced Deep Blue aerosol retrieval algorithm: The second generation, J. Geophys. Res. Atmos., 118(16), 9296–9315, doi:10.1002/jgrd.50712, 2013.

Hyer, E. J., Reid, J. S. and Zhang, J.: An over-land aerosol optical depth data set for data assimilation by filtering, correction, and aggregation of MODIS Collection 5 optical depth retrievals, Atmos. Meas.

Tech., 4(3), 379–408, doi:10.5194/amt-4-379-2011, 2011.

1180 Jia, H., Ma, X., Yu, F. and Quaas, J.: Significant underestimation of radiative forcing by aerosol–cloud interactions derived from satellite-based methods, Nat. Commun., 12(1), 1–11, doi:10.1038/s41467-021-23888-1, 2021.

Journet, E., Balkanski, Y., and Harrison, S. P.: A new data set of soil mineralogy for dust-cycle modeling, Atmos. Chem. Phys., 14, 3801–3816, doi:10.5194/acp-14-3801-2014, 2014.

1185 Kahn, R., Petzold, A., Wendisch, M., Bierwirth, E., Dinter, T., Esselborn, M., Fiebig, M., Heese, B., Knippertz, P., Müller, D., Schladitz, A. and Von Hoyningen-Huene, W.: Desert dust aerosol air mass mapping in the western Sahara, using particle properties derived from space-based multi-angle imaging, Tellus, Ser. B Chem. Phys. Meteorol., 61(1), 239–251, doi:10.1111/j.1600-0889.2008.00398.x, 2009.

Kahn, R. A. and Gaitley, B. J.: An analysis of global aerosol type as retrieved by MISR, J. Geophys. Res.
1190 Atmos., 120(9), 4248–4281, doi:10.1002/2015JD023322, 2015.

Kahn, R. A. and Limbacher, J.: Eyjafjallajökull volcano plume particle-type characterization from space-based multi-angle imaging, Atmos. Chem. Phys., 12(20), 9459–9477, doi:10.5194/acp-12-9459-2012, 2012.

Kalashnikova, O. V. and Kahn, R. A.: Mineral dust plume evolution over the Atlantic from MISR and
1195 MODIS aerosol retrievals, J. Geophys. Res. Atmos., 113(24), 1–17, doi:10.1029/2008JD010083, 2008.

Kaskaoutis, D. G., Rashki, A., Houssos, E. E., Mofidi, A., Goto, D., Bartzokas, A., Francois, P. and Legrand, M.: Meteorological aspects associated with dust storms in the Sistan region, southeastern Iran, Clim. Dyn., 45(1–2), 407–424, doi:10.1007/s00382-014-2208-3, 2015.

Kaufman, Y. J., Tanré, D., Remer, L. A., Vermote, E. F., Chu, A. and Holben, B. N.: Operational remote
1200 sensing of tropospheric aerosol over land from EOS moderate resolution imaging spectroradiometer, J. Geophys. Res. Atmos., 102(D14), 17051–17067, doi:10.1029/96JD03988, 1997.

Kaufman, Y. J., Tanré, D. and Boucher, O.: A satellite view of aerosols in the climate system, Nature, 419(6903), 215–223, doi:10.1038/nature01091, 2002.

King, M. D., Kaufman, Y. J., Tanré, D. and Nakajima, T.: Remote Sensing of Tropospheric Aerosols
1205 from Space: Past, Present, and Future, Bull. Am. Meteorol. Soc., 80(11), 2229–2259, doi:10.1175/1520-0477(1999)080<2229:RSOTAF>2.0.CO;2, 1999.

Kirchstetter, T. W., Novakov, T. and Hobbs, P. V.: Evidence that the spectral dependence of light absorption by aerosols is affected by organic carbon, J. Geophys. Res. Atmos., 109(D21208), doi:10.1029/2004JD004999, 2004.

Knobelspiesse, K., Cairns, B., Ottaviani, M., Ferrare, R., Hair, J., Hostetler, C., Obland, M., Rogers, R., Redemann, J., Shinozuka, Y., Clarke, A., Freitag, S., Howell, S., Kapustin, V. and McNaughton, C.: Combined retrievals of boreal forest fire aerosol properties with a polarimeter and lidar, Atmos. Chem. Phys., 11(14), 7045–7067, doi:10.5194/acp-11-7045-2011, 2011.

Koren, I., Remer, L. A. and Longo, K.: Reversal of trend of biomass burning in the Amazon, Geophys. Res. Lett., 34(20), 2–5, doi:10.1029/2007GL031530, 2007.

Koven, C. D. and Fung, I.: Inferring dust composition from wavelength-dependent absorption in Aerosol Robotic Network (AERONET) data, J. Geophys. Res. Atmos., 111(D14205), doi:10.1029/2005JD006678, 2006.

Krueger, B. J., Grassian, V. H., Cowin, J. P. and Laskin, A.: Heterogeneous chemistry of individual mineral dust particles from different dust source regions: The importance of particle mineralogy, Atmos. Environ., 38(36), 6253–6261, doi:10.1016/j.atmosenv.2004.07.010, 2004.

Lázaro, F. J., Gutiérrez, L., Barrón, V. and Gelado, M. D.: The speciation of iron in desert dust collected in Gran Canaria (Canary Islands): Combined chemical, magnetic and optical analysis, Atmos. Environ., 42(40), 8987–8996, doi:10.1016/j.atmosenv.2008.09.035, 2008.

Lei, Y., Yue, X., Liao, H., Zhang, L., Yang, Y., Zhou, H., Tian, C., Gong, C., Ma, Y., Gao, L. and Cao, Y.: Indirect contributions of global fires to surface ozone through ozone-vegetation feedback, Atmos. Chem. Phys., 21(15), 11531–11543, doi:10.5194/acp-21-11531-2021, 2021.

Lelieveld, J., Berresheim, H., Borrmann, S., Crutzen, P. J., Dentener, F. J., Fischer, H., Feichter, J., Flatau, P. J., Heland, J., Holzinger, R., Korrmann, R., Lawrence, M. G., Levin, Z., Markowicz, K. M., Mihalopoulos, N., Minikin, A., Ramanathan, V., De Reus, M., Roelofs, G. J., Scheeren, H. A., Sciare, J., Schlager, H., Schultz, M., Siegmund, P., Steil, B., Stephanou, E. G., Stier, P., Traub, M., Warneke, C., Williams, J. and Ziereis, H.: Global air pollution crossroads over the Mediterranean, Science (80-.)., 298(5594), 794–799, doi:10.1126/science.1075457, 2002.

Léon, J. F. and Legrand, M.: Mineral dust sources in the surroundings of the North Indian Ocean,

Geophys. Res. Lett., 30(6), doi:10.1029/2002GL016690, 2003.

Lesins, G., Chylek, P. and Lohmann, U.: A study of internal and external mixing scenarios and its effect on aerosol optical properties and direct radiative forcing, J. Geophys. Res. Atmos., 107(D10), doi:10.1029/2001JD000973, 2002.

Letu, H., Nagao, T. M., Nakajima, T. Y., Riedi, J., Ishimoto, H., Baran, A. J., Shang, H., Sekiguchi, M., and Kikuchi, M.: Ice cloud properties from Himawari-8/AHI next-generation geostationary satellite: Capability of the AHI to monitor the DC cloud generation process, IEEE Transactions on Geoscience and Remote Sensing, 57(6), 3229-3239, doi: 10.1109/TGRS.2018.2882803, 2019.

Letu, H., Nakajima, T. Y., Wang, T., Shang, H., Ma, R., Yang, K., Baran, A. J., Riedi, J., Ishimoto, H., Yoshida, M., Shi, C., Khatri, P., Du, Y., Chen, L., and Shi, J.: A new benchmark for surface radiation products over the East Asia–Pacific region retrieved from the Himawari-8/AHI next-generation geostationary satellite, Bulletin of the American Meteorological Society, 103(3), E873-E888, doi: 10.1175/BAMS-D-20-0148.1, 2022.

Levin, Z.: On the interactions of mineral dust, sea-salt particles, and clouds: A measurement and modeling study from the Mediterranean Israeli Dust Experiment campaign, J. Geophys. Res., 110, D20202, doi:10.1029/2005JD005810, 2005.

Levin, Z., Ganor, E. and Gladstein, V.: The effects of desert particles coated with sulfate on rain formation in the Eastern Mediterranean, J. Appl. Meteorol., 35, 1511–1523, 1996.

Levy, R. C., Mattoo, S., Munchak, L. A., Remer, L. A., Sayer, A. M., Patadia, F. and Hsu, N. C.: The Collection 6 MODIS aerosol products over land and ocean, Atmos. Meas. Tech., 6(11), 2989–3034, doi:10.5194/amt-6-2989-2013, 2013.

Li, L., Dubovik, O., Derimian, Y., Schuster, G. L., Lapyonok, T., Litvinov, P., Ducos, F., Fuertes, D., Chen, C., Li, Z., Lopatin, A., Torres, B. and Che, H.: Retrieval of aerosol components directly from satellite and ground-based measurements, Atmos. Chem. Phys., 19(21), 13409–13443, doi:10.5194/acp-19-13409-2019, 2019.

Li, L., Che, H., Derimian, Y., Dubovik, O., Luan, Q., Li, Q., Huang, X., Zhao, H., Gui, K., Zheng, Y., An, L., Sun, T. and Liang, Y.: Climatology of Fine and Coarse Mode Aerosol Optical Thickness Over East and South Asia Derived From POLDER/PARASOL Satellite, J. Geophys. Res. Atmos., 125(16),

doi:10.1029/2020JD032665, 2020a.

Li, L., Che, H., Derimian, Y., Dubovik, O., Schuster, G. L., Chen, C., Li, Q., Wang, Y., Guo, B. and Zhang, X.: Retrievals of fine mode light-absorbing carbonaceous aerosols from POLDER/PARASOL observations over East and South Asia, Remote Sens. Environ., 247, 111913, doi:10.1016/j.rse.2020.111913, 2020b.

Li, L., Che, H., Zhang, X., Chen, C., Chen, X., Gui, K., Liang, Y., Wang, F., Derimian, Y., Fuertes, D., Dubovik, O., Zheng, Y., Zhang, L., Guo, B., Wang, Y. and Zhang, X.: A satellite-measured view of aerosol component content and optical property in a haze-polluted case over North China Plain, Atmos. Res., 266, 105958, doi:10.1016/j.atmosres.2021.105958, 2022.

Li, L., Derimian, Y., Chen, C., Zhang, X., Che, H., Schuster, G. L., Fuertes, D., Litvinov, P., Lapyonok, T., Lopatin, A., Matar, C., Ducos, F., Karol, Y., Torres, B., Gui, K., Zheng, Y., Liang, Y., Lei, Y., Zhu, J., Zhang, L., Zhong, J., Zhang, X., and Dubovik, O.: Dataset used for climatology of aerosol components concentration derived by GRASP algorithm from POLDER-3 observations, Zenodo, https://doi.org/10.5281/zenodo.6395384, 2022.

Li, X. and Strahler, A. H.: Geometric-Optical Bidirectional Reflectance Modeling of the Discrete Crown Vegetation Canopy: Effect of Crown Shape and Mutual Shadowing, IEEE Trans. Geosci. Remote Sens., 30(2), 276–292, doi:10.1109/36.134078, 1992.

Li, Z., Zhao, X., Kahn, R., Mishchenko, M., Remer, L., Lee, K. H., Wang, M., Laszlo, I., Nakajima, T. and Maring, H.: Uncertainties in satellite remote sensing of aerosols and impact on monitoring its long-term trend: A review and perspective, Ann. Geophys., 27(7), 2755–2770, doi:10.5194/angeo-27-2755-2009, 2009.

Li, Z., Gu, X., Wang, L., Li, D., Xie, Y., Li, K., Dubovik, O., Schuster, G., Goloub, P., Zhang, Y., Li, L., Ma, Y. and Xu, H.: Aerosol physical and chemical properties retrieved from ground-based remote sensing measurements during heavy haze days in Beijing winter, Atmos. Chem. Phys., 13(20), 10171–10183, doi:10.5194/acp-13-10171-2013, 2013.

Li, Z., Li, L., Zhang, F., Li, D., Xie, Y. and Xu, H.: Comparison of aerosol properties over Beijing and Kanpur: Optical, physical properties and aerosol component composition retrieved from 12 years ground-based Sun-sky radiometer remote sensing data, J. Geophys. Res. Atmos., 120(4), 1520–1535,

doi:10.1002/2014JD022593, 2015.

Litvinov, P., Hasekamp, O. and Cairns, B.: Models for surface reflection of radiance and polarized radiance: Comparison with airborne multi-angle photopolarimetric measurements and implications for modeling top-of-atmosphere measurements, Remote Sens. Environ., 115(2), 781–792, doi:10.1016/j.rse.2010.11.005, 2011.

Logan, T., Xi, B., Dong, X., Li, Z. and Cribb, M.: Classification and investigation of Asian aerosol absorptive properties, Atmos. Chem. Phys., 13(4), 2253–2265, doi:10.5194/acp-13-2253-2013, 2013.

Logothetis, S.-A., Salamalikis, V., Gkikas, A., Kazadzis, S., Amiridis, V. and Kazantzidis, A.: 15-Year Variability of Desert Dust Optical Depth on Global and Regional Scales, Atmos. Chem. Phys., 1–40, doi:10.5194/acp-2021-418, 2021.

Longtin, D. R., Shettle, E. P., Hummel, J. R., and Pryce, J. D.: A Wind Dependent Desert Aerosol Dust Model: Radiative Properties, Scientific Report No.6, 1988.

Lopatin, A., Dubovik, O., Chaikovsky, A., Goloub, P., Lapyonok, T., Tanré, D. and Litvinov, P.: Enhancement of aerosol characterization using synergy of lidar and Sun- photometer coincident observations : the GARRLiC algorithm, Atmos. Meas. Tech., 6, 2065–2088, doi:10.5194/amt-6-2065-2013, 2013.

Lopatin, A., Dubovik, O., Fuertes, D., Stenchikov, G., Lapyonok, T., Veselovskii, I., Wienhold, F. G., Shevchenko, I., Hu, Q. and Parajuli, S.: Synergy processing of diverse ground-based remote sensing and in situ data using the GRASP algorithm: applications to radiometer, lidar and radiosonde observations, Atmos. Meas. Tech., 14(3), 2575–2614, doi:10.5194/amt-14-2575-2021, 2021.

Lyapustin, A., Wang, Y., Korkin, S. and Huang, D.: MODIS Collection 6 MAIAC algorithm, Atmos. Meas. Tech., 11(10), 5741–5765, doi:10.5194/amt-11-5741-2018, 2018.

Maignan, F., Bréon, F. M., Fédèle, E. and Bouvier, M.: Polarized reflectances of natural surfaces: Spaceborne measurements and analytical modeling, Remote Sens. Environ., 113(12), 2642–2650, doi:10.1016/j.rse.2009.07.022, 2009.

Middleton, N. J.: A geography of dust storms in South-West Asia, J. Climatol., 6(2), 183–196, doi:10.1002/joc.3370060207, 1986.

Mishchenko, M. I. and Geogdzhayev, I. V.: Satellite remote sensing reveals regional tropospheric aerosol

trends, Opt. Express, 15(12), 7423–7438, doi:10.1364/OE.15.007423, 2007.

1320 Mishchenko, M. I. and Travis, L. D.: Satellite retrieval of aerosol properties over the ocean using polarization as well as intensity of reflected sunlight, J. Geophys. Res. Atmos., 102(D14), 16989–17013, doi:10.1029/96JD02425, 1997.

Myhre, G.: Consistency Between Satellite-Derived and Modeled Estimates of the Direct Aerosol Effect, Science (80-.)., 325(5937), 187–190, doi:10.1126/science.1174461, 2009.

1325 Notaro, M., Yu, Y. and Kalashnikova, O. V.: Regime shift in arabian dust activity, triggered by persistent fertile crescent drought, J. Geophys. Res., 120(19), 10229–10249, doi:10.1002/2015JD023855, 2015.

Noyes, K. T. J., Kahn, R. A., Limbacher, J. A., and Li, Z.: Canadian and Alaskan wildfire smoke particle properties, their evolution, and controlling factors, from satellite observations, Atmos. Chem. Phys. Discuss., 1–34, doi: 10.5194/acp-2021-863, 2021.

1330 Pan, X., Ichoku, C., Chin, M., Bian, H., Darmenov, A., Colarco, P., Ellison, L., Kucsera, T., Da Silva, A., Wang, J., Oda, T. and Cui, G.: Six global biomass burning emission datasets: Intercomparison and application in one global aerosol model, Atmos. Chem. Phys., 20(2), 969–994, doi:10.5194/acp-20-969-2020, 2020.

Parol, F., Buriez, J. C., Vanbauce, C., Couvert, P., Sèze, G., Goloub, P. and Cheinet, S.: First results of

1335 the polder „earth radiation budget and clouds" operational algorithm, IEEE Trans. Geosci. Remote Sens., 37(3 II), 1586–1596, doi:10.1109/36.763270, 1999.

Prospero, J. M. and Lamb, P. J.: African Droughts and Dust Transport to the Caribbean: Climate Change Implications, Science (80-.)., 302(5647), 1024–1027, doi:10.1126/science.1089915, 2003.

Prospero, J. M. and Mayol-Bracero, O. L.: Understanding the transport and impact of African dust on the

1340 Caribbean Basin, Bull. Am. Meteorol. Soc., 94(9), 1329–1337, doi:10.1175/BAMS-D-12-00142.1, 2013.

Prospero, J. M., Ginoux, P., Torres, O., Nicholson, S. E. ir Gill, T. E.: Environmental characterization of global sources of atmospheric soil dust identified with the Nimbus 7 Total Ozone Mapping Spectrometer (TOMS) absorbing aerosol product, Rev. Geophys., 40(1), 1–31, doi:10.1029/2000RG000095, 2002.

Qin, W., Zhang, Y., Chen, J., Yu, Q., Cheng, S., Li, W., Liu, X. and Tian, H.: Variation, sources and

1345 historical trend of black carbon in Beijing, China based on ground observation and MERRA-2 reanalysis data, Environ. Pollut., 245(2), 853–863, doi:10.1016/j.envpol.2018.11.063, 2019.

Quaas, J., Jia, H., Smith, C., Albright, A. L., Aas, W., Bellouin, N., Boucher, O., Doutriaux-Boucher, M., Forster, P. M., Grosvenor, D., Jenkins, S., Klimont, Z., Loeb, N. G., Ma, X., Naik, V., Paulot, F., Stier, P., Wild, M., Myhre, G. and Schulz, M.: Robust evidence for reversal in the aerosol effective climate forcing trend, Atmos. Chem. Phys. Discuss., 1–25, doi: 10.5194/acp-2022-295, 2022.

Randerson, J. T., Liu, H., Flanner, M. G., Chambers, S. D., Jin, Y., Hess, P. G., Pfister, G., Mack, M. C., Treseder, K. K., Welp, L. R., Chapin, F. S., Harden, J. W., Goulden, M. L., Lyons, E., Neff, J. C., Schuur, E. A. G. and Zender, C. S.: The impact of boreal forest fire on climate warming, Science (80-.)., 314(5802), 1130–1132, doi:10.1126/science.1132075, 2006.

Randles, C. A., da Silva, A. M., Buchard, V., Colarco, P. R., Darmenov, A., Govindaraju, R., Smirnov, A., Holben, B., Ferrare, R., Hair, J., Shinozuka, Y. and Flynn, C. J.: The MERRA-2 Aerosol Reanalysis, 1980 Onward. Part I: System Description and Data Assimilation Evaluation, J. Clim., 30(17), 6823–6850, doi:10.1175/JCLI-D-16-0609.1, 2017.

Remer, L. A., Kaufman, Y. J., Tanré, D., Mattoo, S., Chu, D. A., Martins, J. V, Li, R.-R., Ichoku, C., Levy, R. C., Kleidman, R. G., Eck, T. F., Vermote, E. and Holben, B. N.: The MODIS Aerosol Algorithm, Products, and Validation, J. Atmos. Sci., 62(4), 947–973, doi:10.1175/JAS3385.1, 2005.

Remer, L. A., Kleidman, R. G., Levy, R. C., Kaufman, Y. J., Tanré, D., Mattoo, S., Martins, J. V., Ichoku, C., Koren, I., Yu, H. and Holben, B. N.: Global aerosol climatology from the MODIS satellite sensors, J. Geophys. Res. Atmos., 113(14), 1–18, doi:10.1029/2007JD009661, 2008.

Remer, L. A., Levy, R. C., Mattoo, S., Tanré, D., Gupta, P., Shi, Y., Sawyer, V., Munchak, L. A., Zhou, Y., Kim, M., Ichoku, C., Patadia, F., Li, R. R., Gassó, S., Kleidman, R. G. and Holben, B. N.: The dark target algorithm for observing the global aerosol system: Past, present, and future, Remote Sens., 12(18), doi:10.3390/RS12182900, 2020.

Román, R., Torres, B., Fuertes, D., Cachorro, V. E., Dubovik, O., Toledano, C., Cazorla, A., Barreto, A., Frutos, A. De and Alados-arboledas, L.: Remote sensing of lunar aureole with a sky camera : Adding information in the nocturnal retrieval of aerosol properties with GRASP code, Remote Sens. Environ., 196, 238–252, doi:10.1016/j.rse.2017.05.013, 2017.

Román, R., Antuña-Sánchez, J., Cachorro, V., Toledano, C., Torres, B., Mateos, D., Fuertes, D., López, C., González, R., Lapionok, T., Dubovik, O. and de Frutos, Á.: Retrieval of aerosol properties using

1375 relative radiance measurements from an all-sky camera, Atmos. Meas. Tech. Discuss., 1–69, doi:10.5194/amt-2021-204, 2021.

Ross, J.: Tasks for vegetation sciences 3: the radiation regime and architecture of plant stands., 1981.

Russell, P. B., Bergstrom, R. W., Shinozuka, Y., Clarke, A. D., Decarlo, P. F., Jimenez, J. L., Livingston, J. M., Redemann, J., Dubovik, O. and Strawa, A.: Absorption Angstrom Exponent in AERONET and
1380 related data as an indicator of aerosol composition, Atmos. Chem. Phys., 10, 1155–1169, doi:10.5194/acp-10-1155-2010, 2010.

Russell, P. B., Kacenelenbogen, M., Livingston, J. M., Hasekamp, O. P., Burton, S. P., Schuster, G. L., Johnson, M. S., Knobelspiesse, K. D., Redemann, J., Ramachandran, S. and Holben, B.: A multiparameter aerosol classification method and its application to retrievals from spaceborne polarimetry, J. Geophys.
1385 Res. Atmos., 119(16), 9838–9863, doi:10.1002/2013JD021411, 2014.

Schepanski, K., Tegen, I. and Macke, A.: Comparison of satellite based observations of Saharan dust source areas, Remote Sens. Environ., 123, 90–97, doi:10.1016/j.rse.2012.03.019, 2012.

Schuster, G., Espinosa, W., Ziemba, L., Beyersdorf, A., Rocha-Lima, A., Anderson, B., Martins, J., Dubovik, O., Ducos, F., Fuertes, D., Lapyonok, T., Shook, M., Derimian, Y. and Moore, R.: A Laboratory
1390 Experiment for the Statistical Evaluation of Aerosol Retrieval (STEAR) Algorithms, Remote Sens., 11(5), 498, doi:10.3390/rs11050498, 2019.

Schuster, G. L., Dubovik, O., Holben, B. N. and Clothiaux, E. E.: Inferring black carbon content and specific absorption from Aerosol Robotic Network (AERONET) aerosol retrievals, J. Geophys. Res., 110, D10S17, doi:10.1029/2004JD004548, 2005.

1395 Schuster, G. L., Dubovik, O. and Arola, A.: Remote sensing of soot carbon - Part 1: Distinguishing different absorbing aerosol species, Atmos. Chem. Phys., 16(3), 1565–1585, doi:10.5194/acp-16-1565-2016, 2016.

Schuster, G. L., Dubovik, O. and Arola, A.: Remote sensing of soot carbon - Part 1: Distinguishing different absorbing aerosol species, Atmos. Chem. Phys., 16, 1565–1585, doi:10.5194/acp-16-1565-
1400 2016, 2016b.

Scollo, S., Kahn, R. A., Nelson, D. L., Coltelli, M., Diner, D. J., Garay, M. J. and Realmuto, V. J.: MISR observations of Etna volcanic plumes, J. Geophys. Res. Atmos., 117(6), 1–13,

doi:10.1029/2011JD016625, 2012.

Shang, H., Chen, L., Letu, H., Zhao, M., Li, S., and Bao, S.: Development of a daytime cloud and haze detection algorithm for Himawari-8 satellite measurements over central and eastern China, Journal of Geophysical Research: Atmospheres, 122, 3528-3543, doi: 10.1002/2016JD025659, 2017.

Shang, H., Letu, H., Pan, X., Wang, Z., Ma, R., Liu, C., Dai, T., Li, S., Chen, L., Chen, C., and Hu, Q.: Diurnal haze variations over the North China plain using measurements from Himawari-8/AHI, Atmospheric Environment, 210, 100-109, doi: 10.1016/j.atmosenv.2019.04.036, 2019.

Schill, G. P., Froyd, K. D., Bian, H., Kupc, A., Williamson, C., Brock, C. A., Ray, E., Hornbrook, R. S., Hills, A. J., Apel, E. C., Chin, M., Colarco, P. R. and Murphy, D. M.: Widespread biomass buring smoke throughout the remote troposphere, 6, 422-427, doi: 10.1038/s41561-020-0586-1, 2020.

Shi, Y., Zhang, J., Reid, J. S., Hyer, E. J., and Hsu, N. C.: Critical evaluation of the MODIS deep blue aerosol optical depth product for data assimilation over North Africa, Atmos. Meas. Tech., 6, 949-969, doi: 10.5194/amt-6-949-2013, 2013.

Shikwambana, L. and Sivakumar, V.: Global distribution of aerosol optical depth in 2015 using CALIPSO level 3 data, J. Atmos. Solar-Terrestrial Phys., 173(December 2017), 150–159, doi:10.1016/j.jastp.2018.04.003, 2018.

Sokolik, I. N. and Toon, O. B.: Incorporation of mineralogical composition into models of the radiative properties of mineral aerosol from UV to IR wavelengths, J. Geophys. Res.-Atmos., 104, 9423–9444, doi:10.1029/1998JD200048, 1999.

Song, Q., Zhang, Z., Yu, H., Ginoux, P. and Shen, J.: Global dust optical depth climatology derived from CALIOP and MODIS aerosol retrievals on decadal timescales: Regional and interannual variability, Atmos. Chem. Phys., 21(17), 13369–13395, doi:10.5194/acp-21-13369-2021, 2021.

Song, Z., Fu, D., Zhang, X., Wu, Y., Xia, X., He, J., Han, X., Zhang, R. and Che, H.: Diurnal and seasonal variability of PM2.5 and AOD in North China plain: Comparison of MERRA-2 products and ground measurements, Atmos. Environ., 191(August), 70–78, doi:10.1016/j.atmosenv.2018.08.012, 2018.

Sullivan, R. C., Moore, M. J. K., Petters, M. D., Kreidenweis, S. M., Roberts, G. C. and Prather, K. A.: Effect of chemical mixing state on the hygroscopicity and cloud nucleation properties of calcium mineral dust particles, Atmos. Chem. Phys., 9(10), 3303–3316, doi:10.5194/acp-9-3303-2009, 2009.

Sun, E., Xu, X., Che, H., Tang, Z., Gui, K., An, L., Lu, C. and Shi, G.: Variation in MERRA-2 aerosol optical depth and absorption aerosol optical depth over China from 1980 to 2017, J. Atmos. Solar-Terrestrial Phys., 186(August 2018), 8–19, doi:10.1016/j.jastp.2019.01.019, 2019.

Sun, H., Biedermann, L., and Bond, T. C.: Color of brown carbon: A model for ultraviolet and visible light absorption by organic carbon aerosol, Geophys. Res. Lett., 34, L17813, doi: 10.1029/2007GL029797, 2007.

Tang, I. N.: Chemical and size effects of hygroscopic aerosols on light scattering coefficients, J. Geophys. Res. Atmos., 101(D14), 19245–19250, doi:10.1029/96JD03003, 1996.

Tang, I. N., Wong, W. T., and Munkelwitz, H. R.: The relative importance of atmospheric sulfates and nitrates in visibility reduction, Atmos. Environ., 15, 2463–2471, 1981.

Tang, M., Cziczo, D. J. and Grassian, V. H.: Interactions of Water with Mineral Dust Aerosol: Water Adsorption, Hygroscopicity, Cloud Condensation, and Ice Nucleation, Chem. Rev., 116(7), 4205–4259, doi:10.1021/acs.chemrev.5b00529, 2016.

Tanré, D., Kaufman, Y. J., Herman, M. and Mattoo, S.: Remote sensing of aerosol properties over oceans using the MODIS/EOS spectral radiances, J. Geophys. Res. Atmos., 102(D14), 16971–16988, doi:10.1029/96JD03437, 1997.

Tanré, D., Bräon, F. M., Deuzä, J. L., Dubovik, O., Ducos, F., Franäois, P., Goloub, P., Herman, M., Lifermann, A. and Waquet, F.: Remote sensing of aerosols by using polarized, directional and spectral measurements within the A-Train: The PARASOL mission, Atmos. Meas. Tech., 4(7), 1383–1395, doi:10.5194/amt-4-1383-2011, 2011.

Titos, G., Ealo, M., Román, R., Cazorla, A., Sola, Y., Dubovik, O., Alastuey, A. and Pandolfi, M.: Retrieval of aerosol properties from ceilometer and photometer measurements: Long-term evaluation with in situ data and statistical analysis at Montsec (southern Pyrenees), Atmos. Meas. Tech., 12(6), 3255–3267, doi:10.5194/amt-12-3255-2019, 2019.

Todd, M. C., Washington, R., Martins, J. V., Dubovik, O., Lizcano, G., M'Bainayel, S. and Engelstaedter, S.: Mineral dust emission from the Bodélé Depression nothern Chad, during BoDEx 2005, J. Geophys. Res. Atmos., 112(6), 1–12, doi:10.1029/2006JD007170, 2007.

Triaud, A. H. M. J.: Earth observation data group: aerosol refractive index archive, available at:

http://eodg.atm.ox.ac.uk/ARIA/data?Minerals/Hematite/(Triaud_2005)/hematite_Triaud_2005.ri (last access: 28 October 2019), 2005.

Tsekeri, A., Lopatin, A., Amiridis, V., Marinou, E., Igloffstein, J., Siomos, N., Solomos, S., Kokkalis, P., Engelmann, R., Baars, H., Gratsea, M. and Raptis, P. I.: GARRLiC and LIRIC : strengths and limitations for the characterization of dust and marine particles along with their mixtures, Atmos. Meas. Tech., 10, 4995–5016, doi:10.5194/amt-10-4995-2017, 2017.

Voss, K. K. and Evan, A. T.: A new satellite-based global climatology of dust aerosol optical depth, J. Appl. Meteorol. Climatol., 59(1), 83–102, doi:10.1175/JAMC-D-19-0194.1, 2020.

Wang, L., Li, Z., Tian, Q., Ma, Y., Zhang, F., Zhang, Y., Li, D., Li, K. and Li, L.: Estimate of aerosol absorbing components of black carbon, brown carbon, and dust from ground-based remote sensing data of sun-sky radiometers, J. Geophys. Res. Atmos., 118(12), 6534–6543, doi:10.1002/jgrd.50356, 2013.

Wang, Z., Lin, L., Xu, Y., Che, H., Zhang, X., Zhang, H., Dong, W., Wang, C., Gui, K. and Xie, B.: Incorrect Asian aerosols affecting the attribution and projection of regional climate change in CMIP6 models, npj Clim. Atmos. Sci., 4(1), 1–8, doi:10.1038/s41612-020-00159-2, 2021.

Washington, R., Todd, M., Middleton, N. J. and Goudie, A. S.: Dust-storm source areas determined by the total ozone monitoring spectrometer and surface observations, Ann. Assoc. Am. Geogr., 93(2), 297–313, doi:10.1111/1467-8306.9302003, 2003.

Van Der Werf, G. R., Randerson, J. T., Giglio, L., Collatz, G. J., Kasibhatla, P. S. and Arellano, A. F.: Interannual variability in global biomass burning emissions from 1997 to 2004, Atmos. Chem. Phys., 6(11), 3423–3441, doi:10.5194/acp-6-3423-2006, 2006.

Wonaschütz, A., Hitzenberger, R., Bauer, H., Pouresmaeil, P., Klatzer, B., Caseiro, A. and Puxbaum, H.: Application of the integrating sphere method to separate the contributions of brown and black carbon in atmospheric aerosols, Environ. Sci. Technol., 43, 1141–1146, doi:10.1021/es8008503, 2009.

Xie, Y., Li, Z., Li, L., Wang, L., Li, D., Chen, C., Li, K. and Xu, H.: Study on influence of different mixing rules on the aerosol components retrieval from ground-based remote sensing measurements, Atmos. Res., 145–146, 267–278, doi:10.1016/j.atmosres.2014.04.006, 2014.

Xie, Y. S., Li, Z. Q., Zhang, Y. X., Zhang, Y., Li, D. H., Li, K. T., Xu, H., Zhang, Y., Wang, Y. Q., Chen, X. F., Schauer, J. J. and Bergin, M.: Estimation of atmospheric aerosol composition from ground-based

remote sensing measurements of Sun-sky radiometer, J. Geophys. Res., 122(1), 498–518, doi:10.1002/2016JD025839, 2017.

Xu, X., Yang, X., Zhu, B., Tang, Z., Wu, H. and Xie, L.: Characteristics of MERRA-2 black carbon variation in east China during 2000–2016, Atmos. Environ., 222(May 2019), 117140, doi:10.1016/j.atmosenv.2019.117140, 2020.

Yu, H., Kaufman, Y. J., Chin, M., Feingold, G., Remer, L. A., Anderson, T. L., Balkanski, Y., Bellouin, N., Boucher, O., Christopher, S., DeCola, P., Kahn, R., Koch, D., Loeb, N., Reddy, M. S., Schulz, M., Takemura, T. and Zhou, M.: A review of measurement-based assessments of the aerosol direct radiative effect and forcing, Atmos. Chem. Phys., 6(3), 613–666, doi:10.5194/acp-6-613-2006, 2006.

Yu, H., Tan, Q., Chin, M., Remer, L. A., Kahn, R. A., Bian, H., Kim, D., Zhang, Z., Yuan, T., Omar, A. H., Winker, D. M., Levy, R. C., Kalashnikova, O., Crepeau, L., Capelle, V. and Chédin, A.: Estimates of African Dust Deposition Along the Trans-Atlantic Transit Using the Decadelong Record of Aerosol Measurements from CALIOP, MODIS, MISR, and IASI, J. Geophys. Res. Atmos., 124(14), 7975–7996, doi:10.1029/2019JD030574, 2019.

Zeng, S., Parol, F., Riedi, J., Cornet, C. and Thieuleux, F.: Examination of POLDER/PARASOL and MODIS/Aqua Cloud Fractions and Properties Representativeness, J. Clim., 24(16), 4435–4450, doi:10.1175/2011JCLI3857.1, 2011.

Zhang, J., Reid, J. S., Westphal, D. L., Baker, N. L., and Hyer, E. J.: A system for operational aerosol optical depth data assimilation over global oceans, Journal of Geophysical Research, 113, D10208, doi: 10.1029/2007JD009065, 2008.

Zhang, Q., Zheng, Y., Tong, D., Shao, M., Wang, S., Zhang, Y., Xu, X., Wang, J., He, H., Liu, W., Ding, Y., Lei, Y., Li, J., Wang, Z., Zhang, X., Wang, Y., Cheng, J., Liu, Y., Shi, Q., Yan, L., Geng, G., Hong, C., Li, M., Liu, F., Zheng, B., Cao, J., Ding, A., Gao, J., Fu, Q., Huo, J., Liu, B., Liu, Z., Yang, F., He, K. and Hao, J.: Drivers of improved PM2.5 air quality in China from 2013 to 2017, Proc. Natl. Acad. Sci. U. S. A., 116(49), 24463–24469, doi:10.1073/pnas.1907956116, 2019.

Zhang, R., Khalizov, A. F., Pagels, J., Zhang, D., Xue, H. and McMurry, P. H.: Variability in morphology, hygroscopicity, and optical properties of soot aerosols during atmospheric processing, Proc. Natl. Acad. Sci., 105(30), 10291–10296, doi:10.1073/pnas.0804860105, 2008a.

515   Zhang, X., Li, L., Chen, C., Chen, X., Dubovik, O., Derimian, Y., Gui, K., Zheng, Y., Zhao, H., Zhang, L., Guo, B., Wang, Y., Holben, B., Che, H. and Zhang, X.: Validation of the aerosol optical property products derived by the GRASP/Component approach from multi-angular polarimetric observations, Atmos. Res., 263, 105802, doi:10.1016/j.atmosres.2021.105802, 2021.

Zhang, X., Li, L., Chen, C., Zheng, Y., Dubovik, O., Derimian, Y., Lopatin, A., Gui, K., Wang, Y., Zhao,

520   H., Liang, Y., Holben, B., Che, H. and Zhang, X.: Extensive characterization of aerosol optical properties and chemical component concentrations: Application of the GRASP/Component approach to long-term AERONET measurements, Sci. Total Environ., 812, 152553, doi:10.1016/j.scitotenv.2021.152553, 2022.

Zhang, X. Y., Gong, S. L., Shen, Z. X., Mei, F. M., Xi, X. X., Liu, L. C., Zhou, Z. J., Wang, D., Wang, Y. Q. and Cheng, Y.: Characterization of soil dust aerosol in China and its transport and distribution

525   during 2001 ACE-Asia: 1. Network observations, J. Geophys. Res. Atmos., 108(9), 1–13, doi:10.1029/2002jd002632, 2003.

Zhang, X. Y., Wang, Y. Q., Zhang, X. C., Guo, W. and Gong, S. L.: Carbonaceous aerosol composition over various regions of China during 2006, J. Geophys. Res. Atmos., 113(14), 1–10, doi:10.1029/2007JD009525, 2008b.

530   Zhang, X. Y., Wang, Y. Q., Niu, T., Zhang, X. C., Gong, S. L., Zhang, Y. M. and Sun, J. Y.: Atmospheric aerosol compositions in China: Spatial/temporal variability, chemical signature, regional haze distribution and comparisons with global aerosols, Atmos. Chem. Phys., 12(2), 779–799, doi:10.5194/acp-12-779-2012, 2012.

Zhang, Y., Li, Z., Sun, Y., Lv, Y. and Xie, Y.: Estimation of atmospheric columnar organic matter (OM)

535   mass concentration from remote sensing measurements of aerosol spectral refractive indices, Atmos. Environ., 179(February), 107–117, doi:10.1016/j.atmosenv.2018.02.010, 2018.